JOURNAL OF GEOPHYSICAL RESEARCH, VOL. 103, NO. B2, PAGES 2563–2584, FEBRUARY 10, 1998

Global magnetization models with a priori information

Michael E. Purucker,[1] Robert A. Langel,[2] Mita Rajaram,[3]
and Carol Raymond [4]

Abstract. In an effort to explore the possible effects of change in integrated magnetization at the continent-ocean boundary and to account for such effects in modeling, an inverse technique is developed which allows for the inclusion of a priori information in models of global crustal magnetization or susceptibility. This technique accounts for processing effects such as main and external field removal. An a priori model consisting of an ocean-continent magnetic contrast, oceanic topography, and remanent magnetization in the Cretaceous quiet zones is constructed using equivalent source dipoles. Previous investigations using similar models utilize only forward modeling procedures. We show how this a priori model can be modified so that the resulting computed field, after removal of spherical harmonics below some specified degree ("main field" removal) and along track filtering ("external field" removal), matches that of the robust POGO-Magsat anomaly map in a least squares sense. The dependence of the final model on the a priori information is also investigated. Between degrees 20 and 60 the final models are found to be almost identical for reasonable a priori conditions. An example from the Gulf of Mexico and surrounding Gulf Coast region serves to illustrate the utility of the technique. High heat flow,> 40° C/km, is observed in much of the Gulf Coast region. The example suggests that the elevated heat flow persists at depth and has elevated the Curie point.

1. Introduction

The outer shell of the Earth, the crust, can be defined [*Meissner*, 1986] on the basis of five different characteristics: (1) seismology, (2) density, (3) rock type, (4) mineralogy, and (5) chemical composition. Each of these characteristics is different for the oceanic and continental crusts. Further, the thickness of the crystalline part of the oceanic crust remains roughly constant from the time of creation in the oceanic ridges to its dissolution at a trench; in contrast, the thickness of the continental crust is more varied, and its average is much greater than that of oceanic crust. Thus a marked magnetic anomaly is anticipated in the relatively abrupt threefold to sixfold thickening of the crust from the oceans to the continents. Satellite observations of the lithospheric magnetic field show little evidence for such anomalies, although *Arkani-Hamed and Strangway* [1986] noted that the continents have relatively stronger magnetic anomalies than do the oceans. This change in magnetic intensity is quantified by *Hinze et al.* [1991].

The lack of distinct and consistent continental-oceanic magnetization contrasts in satellite crustal anomaly maps is attributed either to (1) the removal of these features during spherical harmonic separation of the main field [*Meyer et al.*, 1985; *Counil et al.*, 1991] or (2) the lack of resolution of the signatures in the satellite measurements [*Arkani-Hamed*, 1990]. For example, the signature may be unobservable because of the juxtaposition of gradually thinned continental crust against oceanic crust of normal thickness.

Previous attempts at testing forward models which included long-wavelength features such as a continental-oceanic magnetization contrast yield equivocal results [*Cohen*, 1989; *Cohen and Achache*, 1994]. While some observed anomalies are predicted by this approach, there are also many predicted anomalies that are not observed. Such problems suggest that an inverse approach is required, one in which the a priori long-wavelength features are modified in a least squares sense by the observed anomaly data set.

Our procedure begins with a simple, a priori model of the ocean-continent boundary, termed a "standard Earth magnetization model", version zero, or SEMM-0. This magnetization is then modified until the resulting anomaly pattern, as given in spherical harmonics above some cutoff degree, matches the observed satel-

[1]Raytheon STX, Geodynamics Branch, NASA Goddard Space Flight Center, Greenbelt, Maryland.
[2]NASA Goddard Space Flight Center, Greenbelt, Maryland.
[3]Indian Institute of Geomagnetism, Colaba, Bombay.
[4]Jet Propulsion Laboratory, California Institute of Technology, Pasadena.

Paper number 97JB02935.
0148-0227/98/97JB-02935$09.00

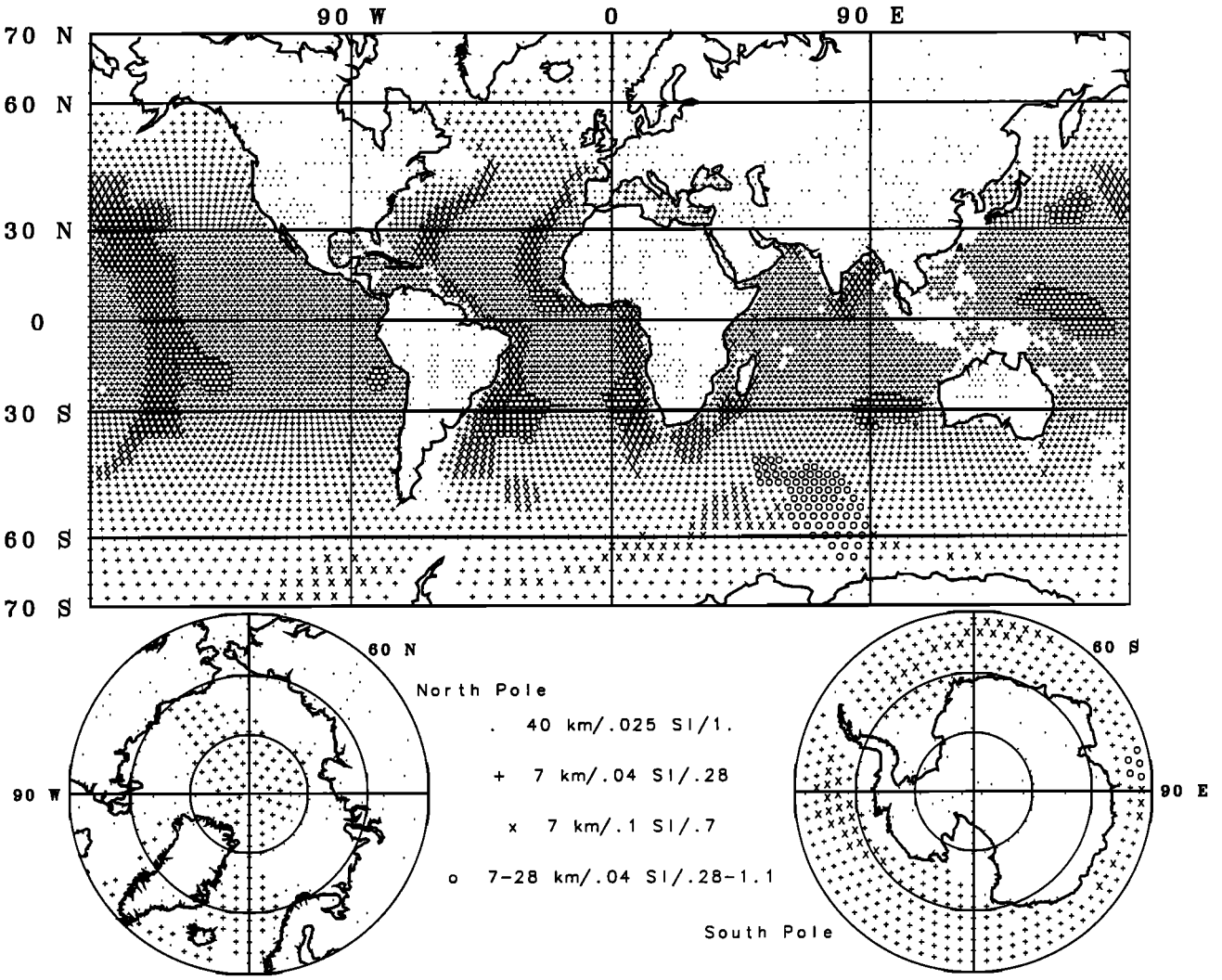

Figure 1. Continental outlines with the positions of the equivalent point dipoles used in this global analysis. Symbols indicate dipole locations by dots in continental crust; plusses in oceanic crust; open circles in oceanic plateaus, and crosses in Cretaceous Quiet Zones. For each symbol at the bottom, the first number is the assumed crustal thickness, followed by the magnetic susceptibility (SI), and the product of the susceptibility times the thickness (ζ). Mercator and polar stereographic projections.

lite magnetic anomaly map. Because the observed map includes spherical harmonics above degree 15, the cut-off degree for the SEMM-0 is taken to be degree 15. The crustal magnetization model is then the sum of the SEMM-0 and the necessary modifications. The process is iterative but convergent, includes the difference between oceanic and continental crust, and is adaptable to local analysis. As with other interpretive methods for magnetic field data, the results are nonunique.

The observed satellite magnetic anomaly map chosen for this purpose is one which retains only the common features of the POGO [*Langel*, 1990] and Magsat [*Ravat et al.*, 1995] maps [*Arkani-Hamed et al.*, 1994; *Purucker et al.*, 1996]. The standard deviations of the chosen map are mostly less than 1 nT at low and mid-latitudes but can be as large as 4 nT over the auroral belts [*Arkani-Hamed et al.*, 1994, Figure 8b]. Of a total of 219 magnetic anomalies identified in the POGO and Magsat anomaly maps, only four significant (in excess of 4 nT) anomalies are present in only one of the maps [*Purucker and Langel*, 1996]. This consistency testifies to the reproducibility of the anomalies and to their origin in the lithosphere.

2. A Standard Earth Magnetization Model

To define the SEMM-0, the continental margin is placed at the 1 km bathymetric contour, typically along the continental slope, as given by *Row et al.* [1995]. Values of susceptibility are assigned to continental and oceanic crust and remanent magnetization to Cretaceous Quiet Zones (KQZ) within oceanic crust. The model takes the form of 11,562 equivalent point dipoles

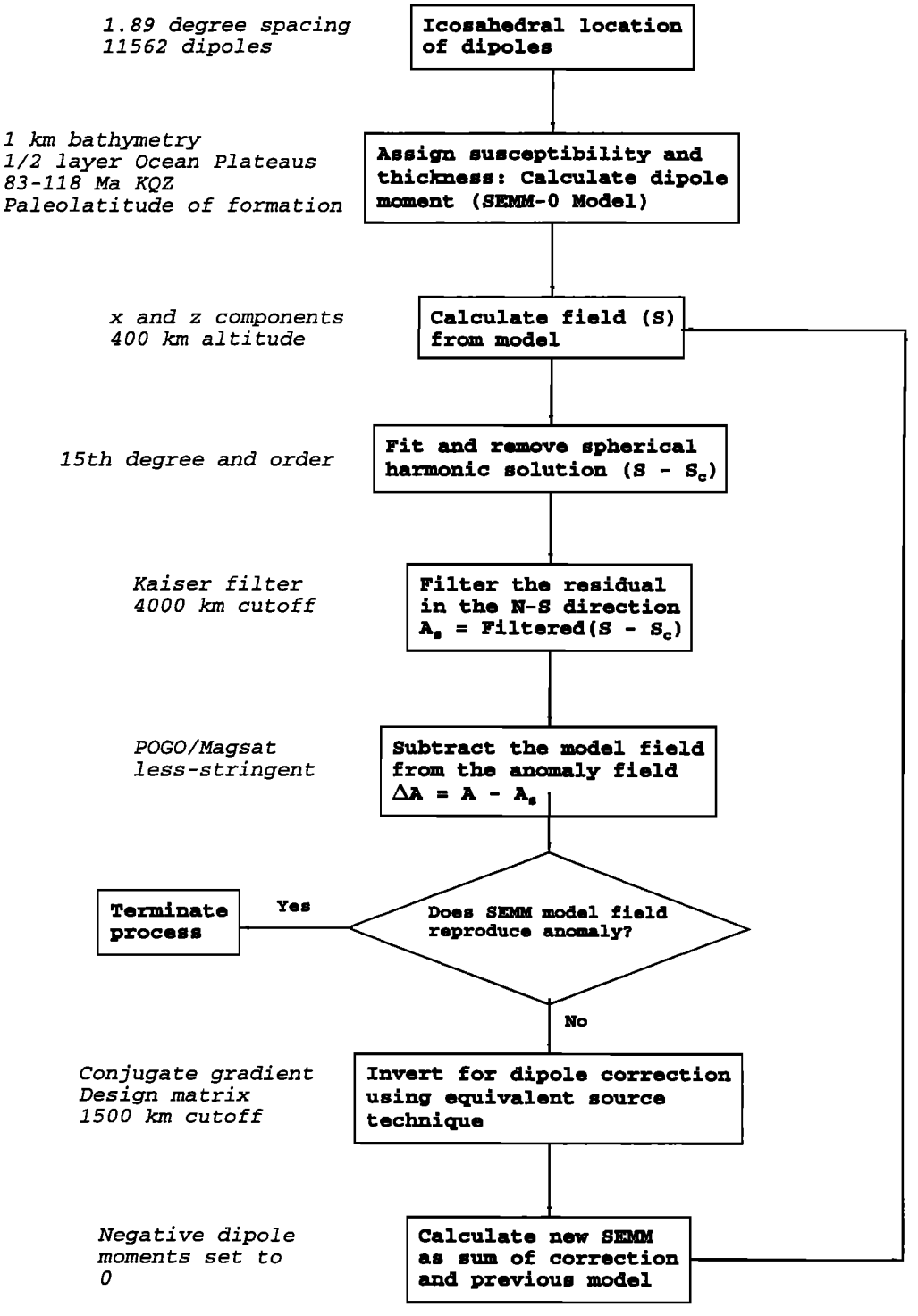

Figure 2. Block diagram of the derivation of the global magnetic model.

[*Langel and Hinze*, 1998], each representing a region equal to a 1.89° × 1.89° area at the equator. Except in the KQZ, as discussed below, magnetization direction is assumed to be along the direction of the ambient main field. Figure 1 is a plot of the position of all the equivalent point dipoles used in this global calculation with symbols identifying the assumed type of crust.

The procedure to develop a SEMM model is detailed in Figure 2. The magnetic vector field **S** from the SEMM-0 magnetization distribution is fitted with a 15th degree and order spherical harmonic model. Subtracting the resulting model field, $\mathbf{S_C}$, from **S** corresponds to the step of removing a model of the Earth's main field from the measured satellite data to obtain residuals corresponding to the lithospheric field. In order to remove external fields like the ring current, the satellite residual field is normally filtered along the track of the orbit [*Ravat et al.*, 1995]. Correspondingly, the

residual, $\mathbf{A_{S'}} = \mathbf{S} - \mathbf{S_C}$, is filtered in the north-south direction. To first order, this is an effective and simplifying strategy for polar-orbiting satellites such as Magsat and POGO. The resulting filtered difference field, $\mathbf{A_S}$, corresponds to the "measured" anomaly field and is called the anomaly field of the SEMM-0,

$$\mathbf{A_S} = Filtered(\mathbf{S} - \mathbf{S_C}). \quad (1)$$

Then the magnetization distribution specified in the SEMM-0 is modified until the resulting anomaly pattern, with the spherical harmonic model removed, matches the satellite-derived magnetic anomaly map $\mathbf{A}$. To accomplish this task a modified data set is created by subtracting $\mathbf{A_S}$ from the anomaly field $\mathbf{A}$

$$\Delta\mathbf{A} = \mathbf{A} - \mathbf{A_S}. \quad (2)$$

Then a set of dipole modifications is derived that reproduces $\Delta\mathbf{A}$ in a least squares sense [*Purucker et al.*, 1996]. The new model, called SEMM-1, is the sum of these corrections and the dipoles of the SEMM-0.

In 1% of the dipoles, the correction resulted in a negative value. A negative effective susceptibility might be expected over oceanic zones with reversed remanance or over continental areas with extensive reversely magnetized rocks (D. Ravat, personal communication, 1996). Because there is no consensus on this point, we have elected to set negative values to 0 (a positivity constraint). This positivity constraint can be relaxed to allow for reversed remanence.

The north (ΔX) and vertical (ΔZ) components of the vector $\mathbf{A}$ are used in the spherical harmonic and equivalent source fitting because of the problems inherent in using the total field to define source functions over the magnetic equator [*Mayhew et al.*, 1980; *Purucker*, 1990]. These components are calculated from a modified version of the magnetization contrast map presented as Figure 2 of *Purucker et al.* [1996]. The only modification, over northern Argentina, was done because the published magnetization solution there is found to be more highly variable than the gently varying total field map from which it was generated. The modification entailed decreasing the number of iterations of the conjugate gradient technique in order to produce a smoother variation in magnetization.

3. Beginning Model

3.1. Choice of Susceptibility and Thickness

What is a realistic a priori susceptibility for the continental and oceanic lithosphere? Since susceptibility and permanent magnetization in the direction of the inducing field cannot be distinguished, we refer to their collective sum as susceptibility. Compilations of magnetic susceptibility [*Clark*, 1991] in continental igneous and metamorphic rocks show a wide range, with an average value in the range of 0.005 to 0.1 SI. If we assume that lower crustal rocks are mafic granulites [*Wasilewski and Mayhew*, 1992], then average values of 0.02 to 0.07 SI might be expected [*Clark*, 1991]. Here, the value of 0.05 SI in a lower continental crust of thickness 20 km is adopted for the starting model. This is equivalent to a susceptibility of 0.025 SI over the entire crustal thickness of 40 km.

For oceanic areas, an average susceptibility of 0.040 SI in a 7 km thick crust is adopted. Because the uppermost oceanic mantle may also possess magnetic properties, the selected crustal thickness is greater than the more realistic value of 5 km [*Thomas*, 1987]. Some authors [*Toft and Arkani-Hamed*, 1992; *Cohen and Achache*, 1994] argue for significant magnetizations in the uppermost mantle because of the high magnetizations required if only the oceanic crust is assumed magnetic. Two other factors are relevant to the selection of starting values. The contrast assumed in this study, 23,000 Amperes in an inducing field of 40,000 nT, falls within the range (22,000-37,000 A) determined in previous studies of the ocean-continent bulk magnetization contrast [*Arkani-Hamed and Dyment*, 1996]. A positivity constraint was also applied to the product of the susceptibility times thickness as noted in section 2. By trial and error it was found that the values adopted for oceanic susceptibility and thickness are the minimum required to prevent more than a small (1%) fraction of the dipoles from becoming negative after correction. Models with more extreme values are explored in a sensitivity study in section 6.

3.2. Refinements in the Oceanic Realm

In most oceanic regions, fields from the alternating normal and reverse remanent magnetizations of the oceanic seafloor spreading magnetic anomalies are nearly cancelled at satellite altitude. However, coherently magnetized oceanic crust associated with the KQZ is extensive enough to result in measurable anomalous field at satellite altitude [*LaBrecque and Raymond*, 1985; *Hayling and Harrison*, 1986; *Toft and Arkani-Hamed*, 1992]. Accordingly the KQZ oceanic crust, identified by taking the 83 and 118 Ma boundaries [*Harland et al.*, 1989] in the digital age grid of *Mueller et al.* [1993], is treated separately in the SEMM. Dipoles that lay within the KQZ are assigned an initial magnetization of 3.3 A/m, equivalent to a susceptibility of 0.1 SI in an ambient field of 42,000 nT. Also, because KQZ crust in the western Pacific was formed at significantly lower latitudes than its present position [*Petronotis et al.*, 1992; *Vasas et al.*, 1994], dipoles in the KQZ are assigned an inclination corresponding to their estimated paleolatitude of formation, rather than the inclination of the present-day field. The terrane immediately to the east and north of the Tonga trench, considered by some authors [*Toft and Arkani-Hamed*, 1992; *Cohen and Achache*, 1994] to be part of the KQZ, is considered by the authors of the digital age map [*Mueller et al.*, 1993] to be an area with insufficient data coverage. We have adopted this more conservative approach and have not included this area as part of the KQZ. With the exception of the oceanic regions discussed here, no attempt is made to account for permanent magnetizations in directions oblique to the main geomagnetic field. In

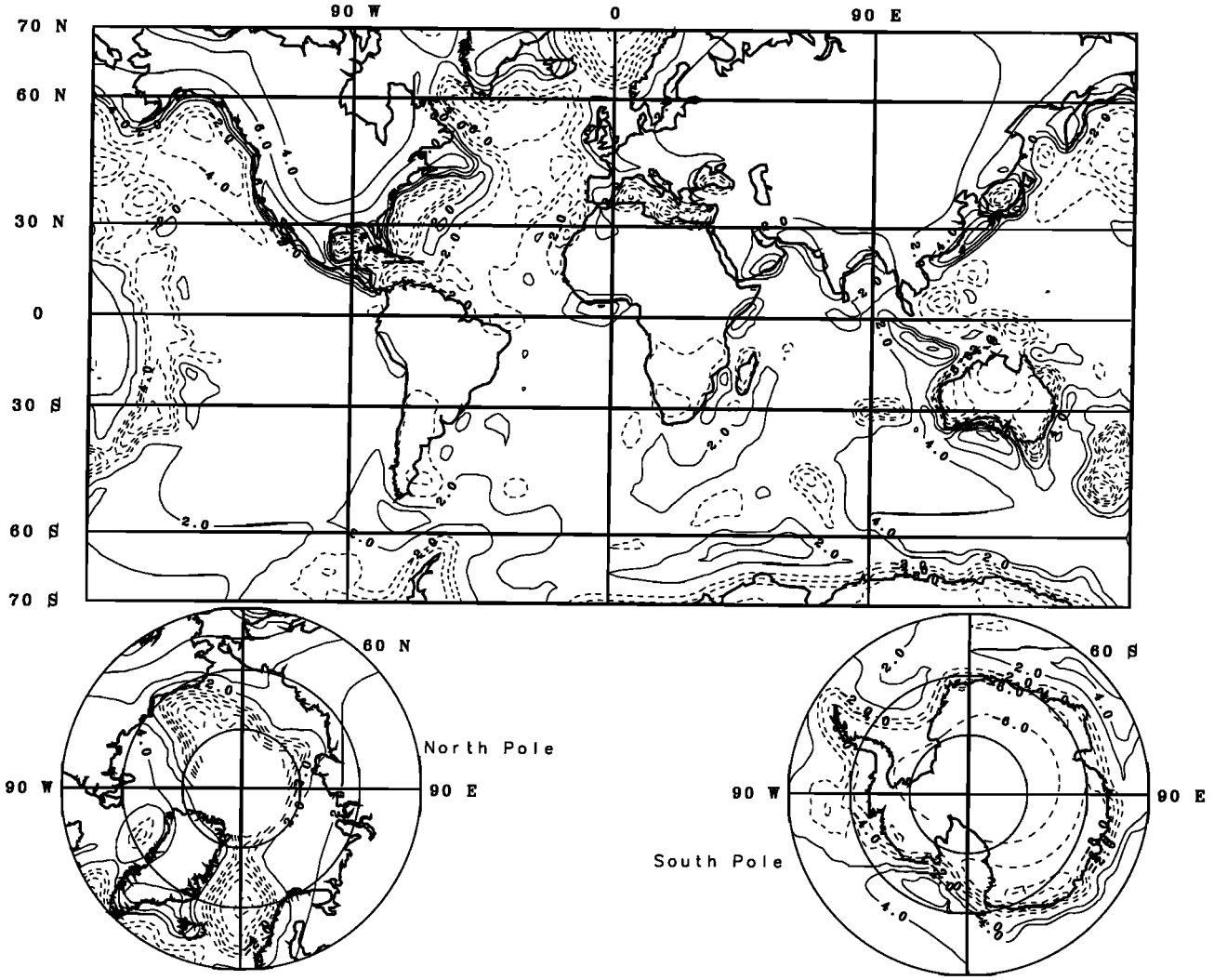

Figure 3a. Vertical field Z, at 400 km based on the SEMM-0 model for all spherical harmonic degrees. The contour interval is 2 nT. Negative values are dashed. The 0 nT contour is not plotted. Mercator and polar stereographic projections.

the context of these calculations, a more sophisticated model, such as that of *Carrizo* [1994], is not feasible.

In order to account for the thicker crust of the oceanic plateaus, they are included as distinct features, in much the same way as they were modeled in the work of *Toft and Arkani- Hamed* [1992] and *Cohen and Achache* [1994]. The oceanic plateaus from *Sandwell and MacKenzie* [1989] and *Marks and Sandwell* [1991] are adopted in this study. The plateaus are assumed to have oceanic crustal susceptibility values, except that their crustal thicknesses are computed using an Airy compensation model. Oceanic plateaus are the shortest-wavelength a priori feature of the SEMM-0 and have minimal influence on the final magnetic model. Because of this and the complications inherent in their modeling, they are probably best interpreted on a case-by-case basis.

3.3. Summary of the SEMM-0

The adopted SEMM-0 results in a starting model with dipole locations and attributes as summarized in Figure 1. The physical quantity inferred is the integrated magnetization, in this case the susceptibility times the thickness, herein denoted as ζ. Figure 3a shows the vertical component of the magnetic field, Z, produced by the a priori model. Figure 3b shows the residual Z field after subtraction of the field from the spherical harmonic model. Figure 4 shows the result after the north-south filter is applied to the data of Figure 3b.

The SEMM-0 is an oversimplification of actual crustal properties, particularly for continental crust. Its purpose is to introduce possible effects of large-scale magnetization differences between continental and oceanic crust. It is anticipated that this contrast is not everywhere the same, nor everywhere a sharp discontinuity, as portrayed in the model. Although the long-wavelength characteristics of the model are inaccessible to correction by available data, the short-wavelength effects in Figure 4 can be compared with satellite data, and adjustments can be made to bring the two into

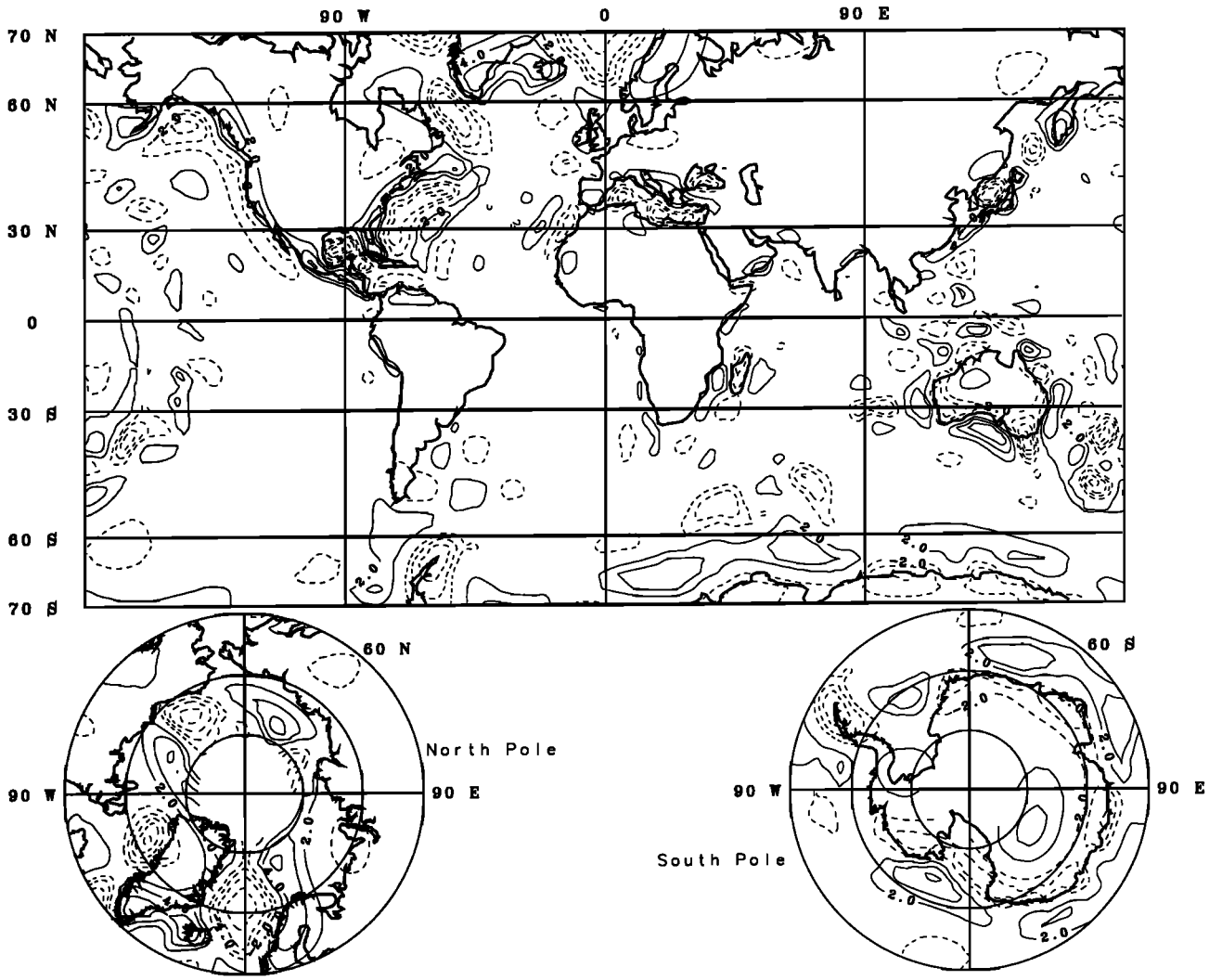

Figure 3b. Same as Figure 3a, except for spherical harmonic degree > 15.

agreement. However, the short-wavelength result may not represent the true magnetization, as will be discussed in section 6.

4. Implications of the SEMM-0

A careful inspection of Figure 3a shows a significant continent-ocean contrast in the model anomaly pattern. A contrast is also seen at the boundaries of the KQZ. In the portion of the field of degree >15 (Figure 3b), most of the continent-ocean contrast is removed, but short-wavelength anomalies still outline many of the boundaries. Many of these "edge" anomalies have substantial north-south trends that are effectively removed by the applied filter. The residual field (Figure 4) reveals a few localized and elongate anomalies, mainly in coastal regions. These observations support the results of *Meyer et al.* [1985], *Cohen* [1989], and *Counil et al.* [1991] that most of the continent-ocean contrast is contained in the low degree field and is removed along with the main field when residuals are computed relative to a main field model and when along-track filtering is applied to the data.

The residual field (in Figure 4) is the filtered short-wavelength portion of the field from the contrasting continental vs. oceanic and oceanic vs. KQZ magnetizations of the SEMM-0. To the degree that the regional contrasts in the SEMM-0 correspond to ground truth, the resulting anomalies should be found in the maps derived from measured data. Figure 5 shows the vertical component anomaly map (ΔZ) derived from the combined POGO-Magsat magnetic anomaly map of *Arkani-Hamed et al.* [1994], and Figure 6 shows a map of the correlation coefficient between the map of Figure 4 and that of Figure 5.

Examination of these maps indicates substantial regions of positive correlation between the SEMM-0 anomalies and the measured anomalies, most commonly in the oceanic regime near passive margins. Amplitudes are often within a factor of 0.7. Not all coasts show such anomalies, nor do all SEMM-0 anomalies correlate well with the measured anomalies.

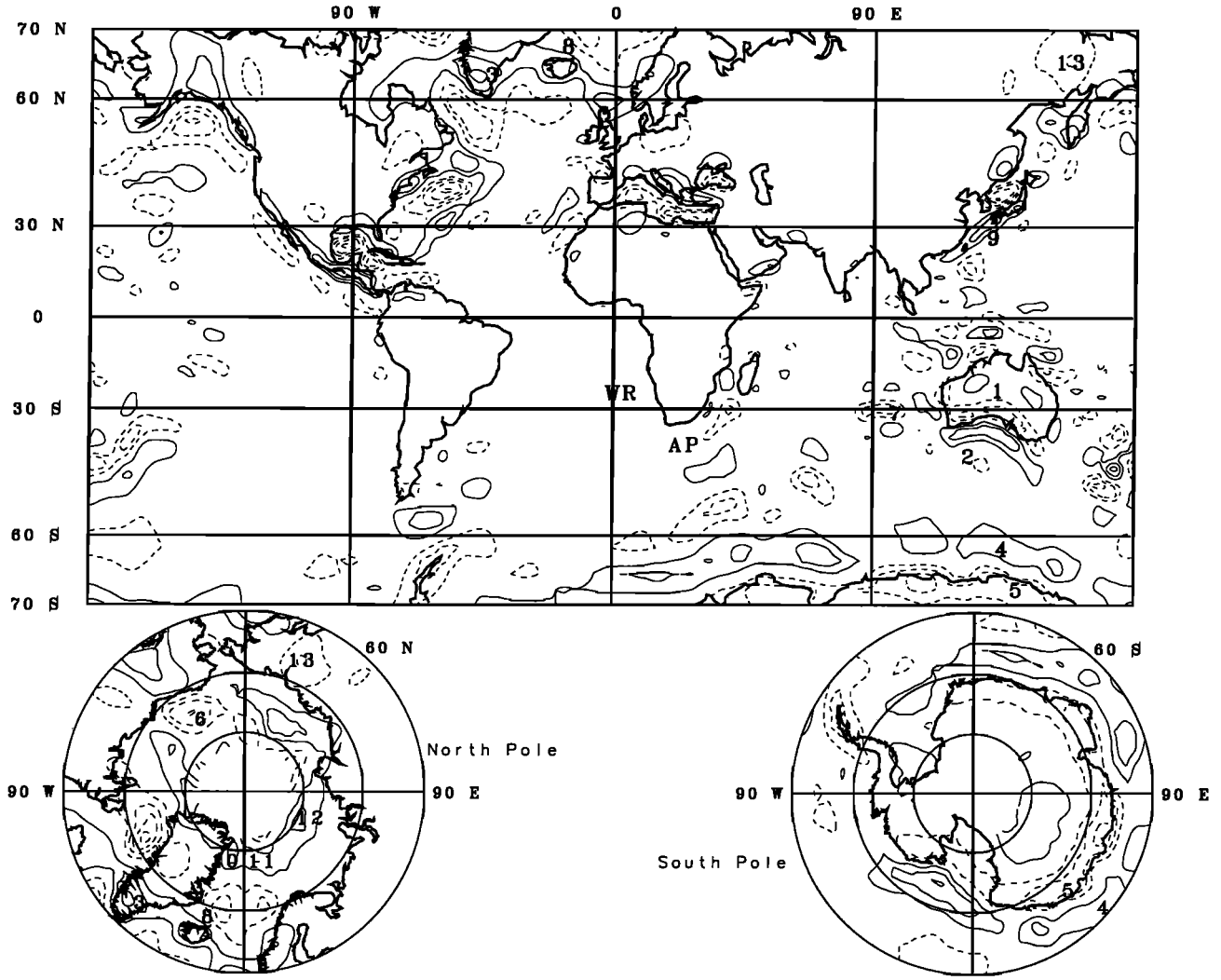

Figure 4. North-south filtering, corresponding to removal of external field, from vertical field Z of Figure 3b. The contour interval is 2 nT. Negative values are dashed. The 0 nT contour is not plotted. Mercator and stereographic projections. The numbered values are discussed in the text. WR, Walvis Ridge; AP, Aguhlas Plateau.

4.1. Comparison With Previous Work

Toft and Arkani-Hamed [1992] use a forward modeling approach to model the magnetic fields expected over the KQZ and oceanic plateaus of the Pacific. Although they do not include a continent-ocean contrast in their flat-Earth approximation, they do use a high-pass filter to remove wavelengths longer than 2800 km from their model. The synthetic anomalies generated by their model are similar to those generated by the SEMM-0. The exception is in the area north and east of the Tonga trench which, as previously noted, is not considered part of the KQZ in our model.

Cohen and Achache [1994] develop a forward model that contains many of the same elements as our SEMM-0. Their initial step is that of a continent-ocean contrast like that described by *Counil et al.* [1991]. Further steps include (1) assumption of oceanic upper mantle induced magnetization down to a Curie isotherm, taken to be 600° C, which deepens with the age of the crust, (2) accounting for residual oceanic topography from that expected from subsidence, which mostly is associated with oceanic plateaus, and (3) assumption of remanent magnetization in the KQZ. The continent-ocean contrast, increased magnetization in oceanic plateaus, and magnetization of the KQZ are very much like the assumptions built into the SEMM-0. It is thus expected that the synthetic anomalies from their model and from the SEMM-0 should be very similar. A comparison indicates that synthetic anomalies along coastlines are indeed very similar. Taking into account the restricted latitudinal range of *Cohen and Achache* [1994], in excess of 80% of the anomalies greater than 2 nT correlate between Plate 8 of *Cohen and Achache* [1994] and our Figure 4. The differences relate mainly to the assignment of complicated margins to continental or oceanic affinity. Examples where differences exist include the Gulf of Mexico, the Mediterranean and Black Seas, and the Gulf of Japan. Our model assigns these seas to oceanic affinity where depths in excess of 1 km occur.

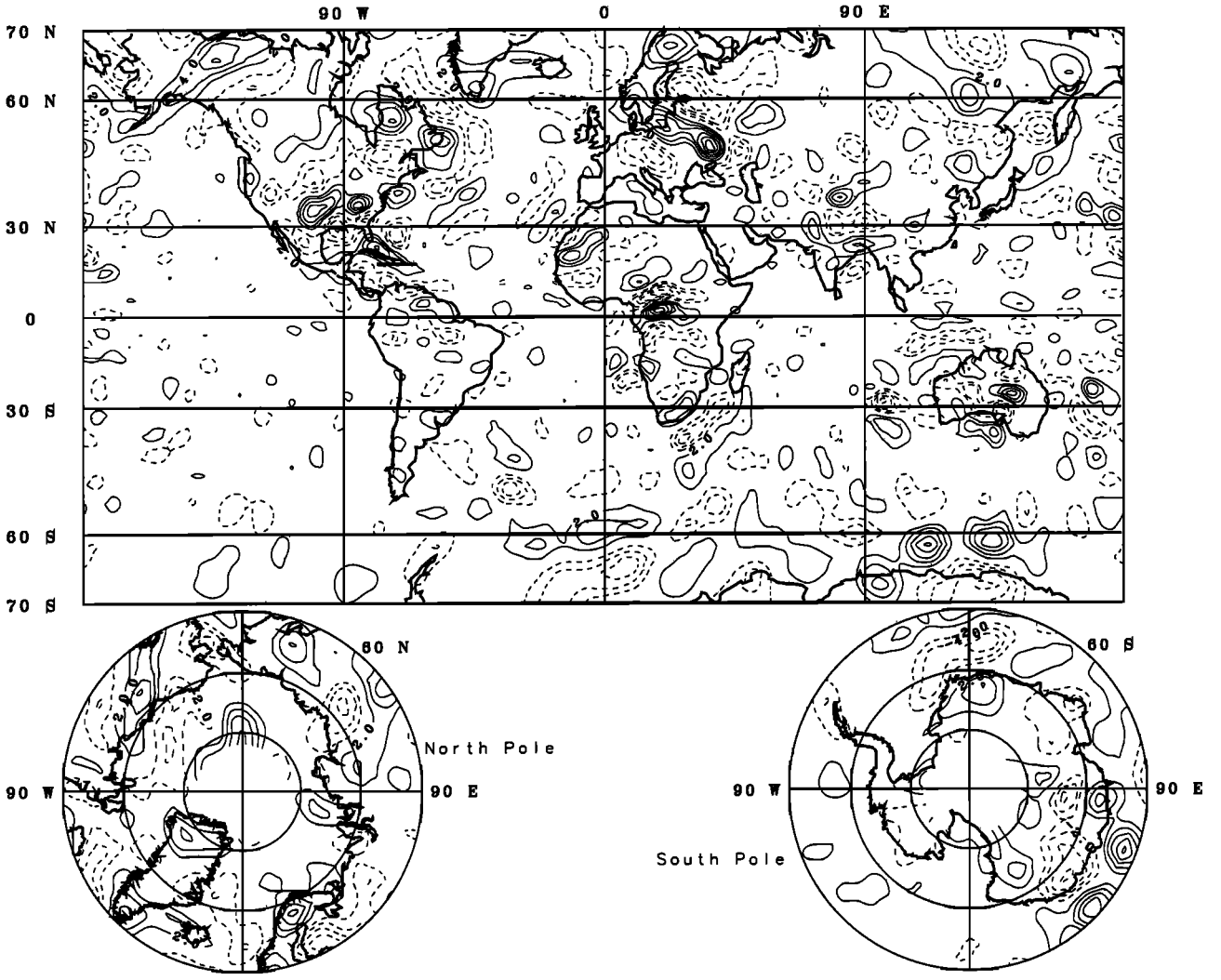

Figure 5. Measured vertical component anomaly map (ΔZ) from the combined POGO and Magsat satellite anomaly model. The contour interval is 2 nT. Negative values are dashed. The 0 nT contour is not plotted. Mercator and stereographic projections. The less stringent model of *Arkani-Hamed et al.* [1994] was inverted to a magnetization contrast map using the techniques outlined by *Purucker et al.* [1996]. The magnetization contrast map was then used to calculate the vertical component anomaly map shown here.

4.2. Application of SEMM-0 and 3SMAC

Neither the model of *Cohen and Achache* [1994] nor our model successfully matches the anomaly pattern seen in the observations over the Gulf of Mexico. Because the Gulf of Mexico is an example of a complicated margin, the derivation of realistic simple models such as the SEMM-0 or the model of *Cohen and Achache* [1994] might be expected to be difficult. If this margin is modeled in the most realistic way possible, do the observed anomalies and the model anomalies agree? In order to address this question, let us examine a global model that contains many of the elements necessary to construct a more realistic forward model. This is the 3SMAC model of *Nataf and Ricard* [1996], designed not for magnetics but for seismic tomography. This new model deserves further study. The model contains estimates of the thickness of the igneous and sedimentary crust on a 2 degree grid worldwide and also a tectonic regionalization from which to predict heat flow and hence an estimate of the Curie point isotherm. The model also contains a subdivision of the crust into oceanic and continental realms. In order to calculate the thickness of the magnetic crust from the 3SMAC model, the igneous crustal thickness is reduced by that portion which has a temperature greater than the Curie point of magnetite, taken to be 570° C. The weaknesses of the model are (1) the inadequate and uneven distribution of information about the thickness of the igneous and sedimentary crust and (2) the coarseness of the tectonic regionalization used to predict heat flow.

In a region centered on the Gulf of Mexico, the thickness of the igneous crust from the 3SMAC model is

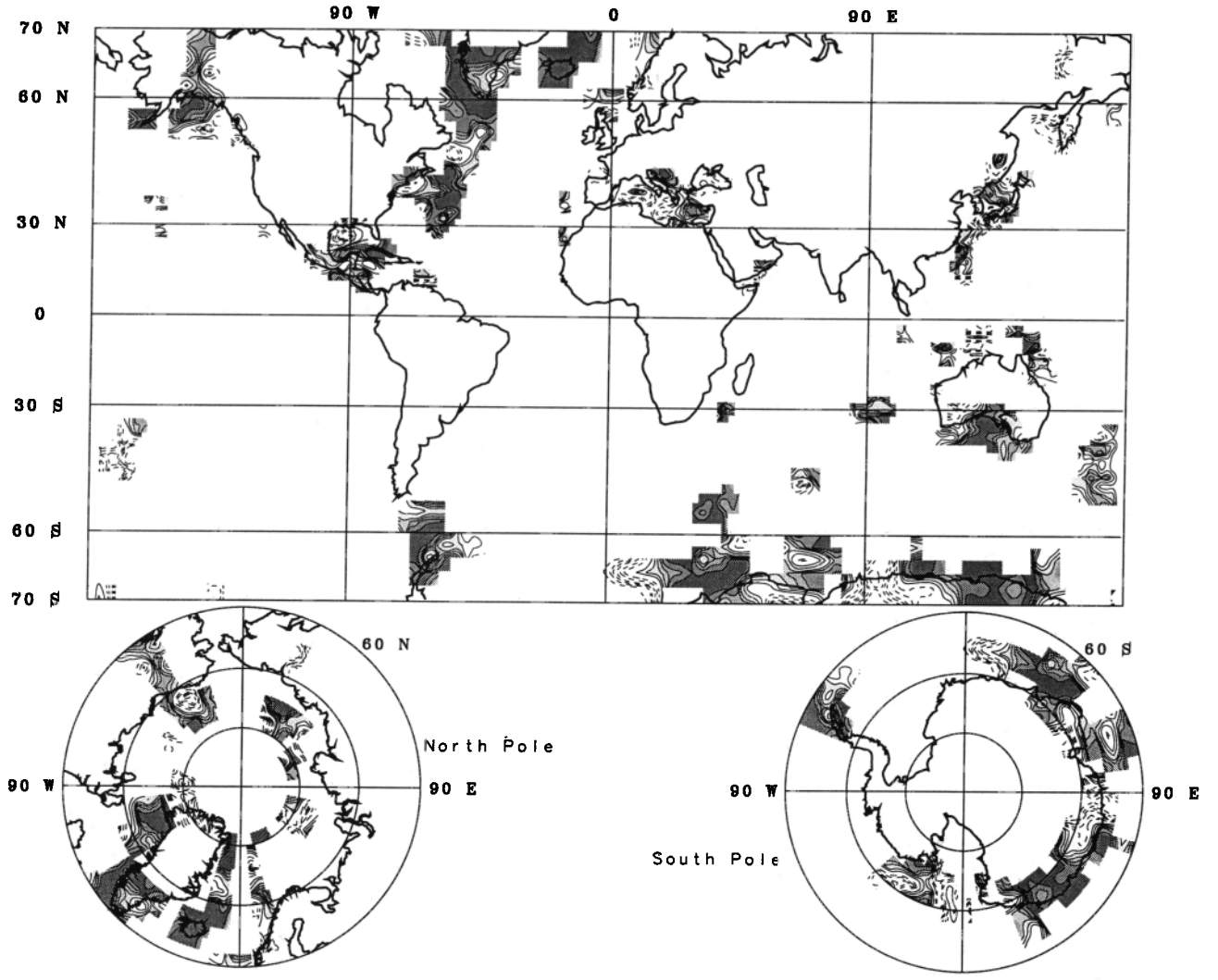

Figure 6. Correlation between the calculated SEMM-0 field of Figure 4 and the measured anomalies of Figure 5. The correlation is computed only for regions where SEMM-0 anomalies exceed 4 nT in magnitude. For a particular location, the correlation coefficient is computed based on overlapping regions of 5° latitude by 5° longitude centered on that location. Contour levels are ± 0.2, 0.4, 0.6, 0.8, and 0.9. Dashed lines are negative correlations; positive correlations in excess of 0.2 are shaded, with darker shades representing higher correlations. Mércator and polar stereographic projections.

shown (Figure 7a). Mexico, Florida, the Gulf Coast, and parts of the western United States are considered tectonic regions with a model heat flow and geotherm in the 3SMAC. This geotherm predicts a Curie point isotherm at 29 km depth (pluses, Figure 7b). The remainder of the continental regions shown in Figure 7b are considered stable platforms with an estimated Curie point isotherm at 58 km depth (circles, Figure 7b). Figure 7c shows the thickness of the sedimentary sequence, estimated at nearly 18 km in the offshore Mississippi River delta. The thickness of the magnetic crust (Figure 7d) differs significantly from the igneous crust thickness in the western United States due to the shallow Curie point isotherm there. Over the Gulf Coast a slight change from the igneous crustal thickness is noted because of the thick sedimentary cover. Assigning the same continental and oceanic susceptibilities as assigned in the SEMM-0, the vertical field (Figure 8a) was calculated and processed in the same way as in the SEMM-0. This vertical field can be compared to that predicted by the SEMM-0 (Figure 8b) and the observed vertical field (Figure 8c). Also included is an estimate of the error in the observed scalar or total field (Figure 8d)(taken from Figure 8b of *Arkani-Hamed et al.* [1994]). Signal/noise ratios in excess of 5/1 are associated with the major magnetic anomalies. The location and magnitude of the observed low over the Gulf of Mexico and adjacent Louisiana coastal plain are better modeled in the 3SMAC model than in the SEMM-0 model. The better correspondence is due to (1) the gradational character of the continental-oceanic boundary in the 3SMAC model and (2) the reduction in the mag-

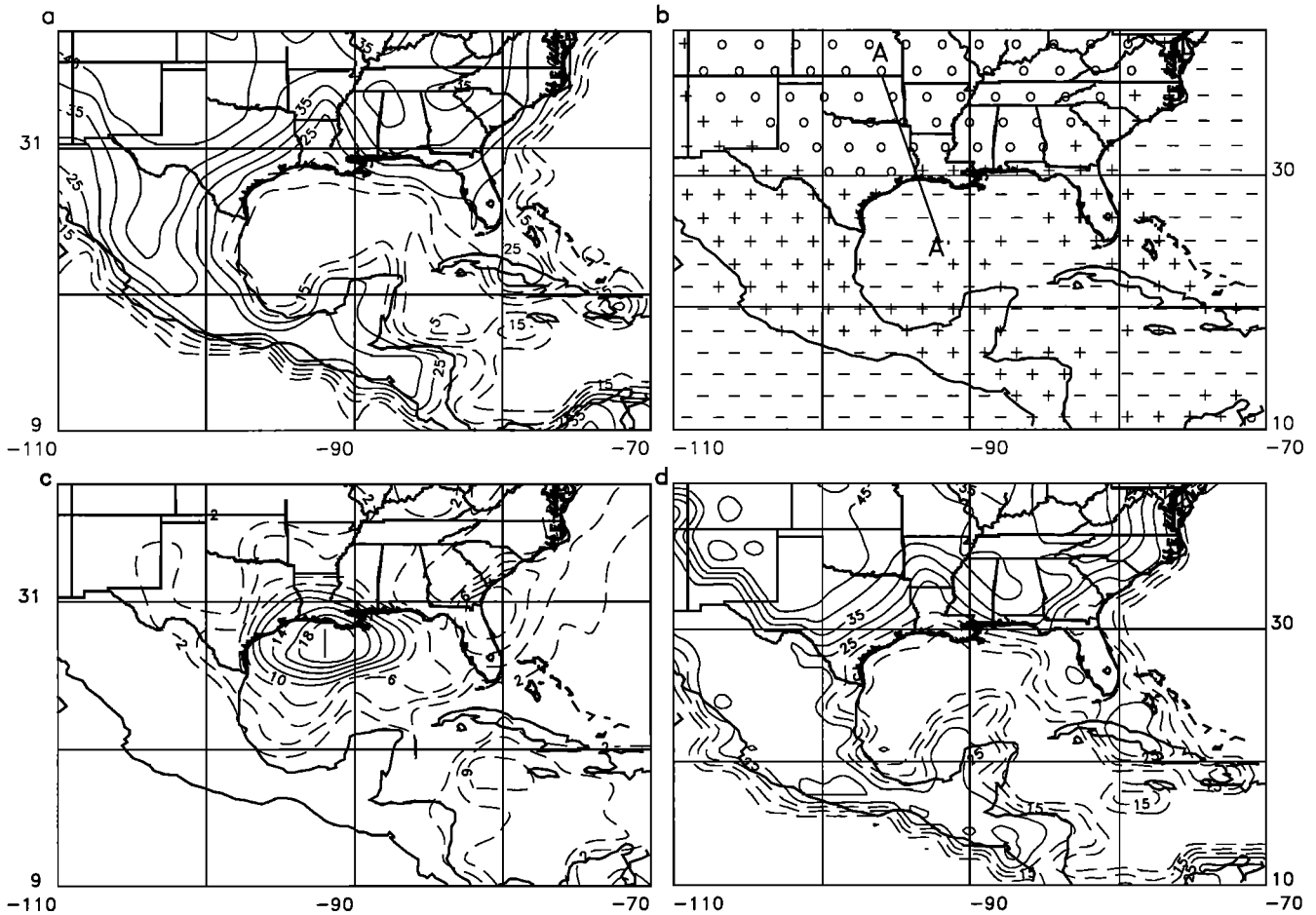

Figure 7. Maps showing features of the 3SMAC [*Nataf and Ricard*, 1996] model over the Gulf of Mexico and surrounding region. (a) The thickness (in km) of the igneous crust below the sediments. The contour interval is 5 km. Thicknesses $\leq$ 20 km are dashed. (b) The tectonic regionalization from which the geotherm is estimated. Symbols indicate dipole locations by circles in stable platforms, plusses in tectonic regions, and minuses in oceanic areas. The A-A' line locates the cross section of Figure 12. (c) A map of sedimentary thickness (in km). The contour interval is 2 km. Thicknesses < 10 km are dashed. (d) The thickness (in km) of the crustal magnetic layer from the 3SMAC model. This thickness is calculated by reducing the igneous crustal thickness where temperatures exceed the Curie temperature. The contour interval is 5 km. Thickness < 25 km are dashed. All figures use a Mercator projection.

netic crustal thickness over the Gulf Coast because of the thick sedimentary cover. Current crustal models of the Gulf of Mexico [*Sawyer et al.*, 1991] are similar but more detailed than the 3SMAC model.

There remains a discrepancy between the 3SMAC model and the observations. The center of the low in the observations is about 250 km north of the low in the 3SMAC and slightly more intense. This discrepancy will be explored further in section 7.

4.3. Correlation With Observations

The SEMM-0 a priori is an approximation in the sense that it is inferred, not measured. So the correlations shown (Figure 6) should be taken as indicative, not definitive. In the following discussion of these correlations, the anomaly numbers refer to the numbers in Figure 4.

1. Anomalies at coastlines may reflect the continent-ocean contrast rather than local variations in magnetization. For example, the measured low-high anomaly pair at the south coast of Australia, corresponding to anomalies 1 and 2, may not indicate locally high onshore magnetization. Similarly, the positive field at the southern tip of Greenland, corresponding to anomaly 3, may not indicate higher magnetization in that portion of the Greenland crust. Similar considerations apply to portions of the Antarctic margins (e.g., anomalies 4 and 5) and to the north coast of Alaska (e.g., anomaly 6). Note that the field values shown on Figure 4 are the vertical field (Z), not the total or scalar field.

2. Anomalies associated with some oceanic plateaus can be accounted for with the SEMM assumption of thickened crust and, in some cases, enhanced KQZ magnetization, as, for example, Broken Ridge (Anomaly

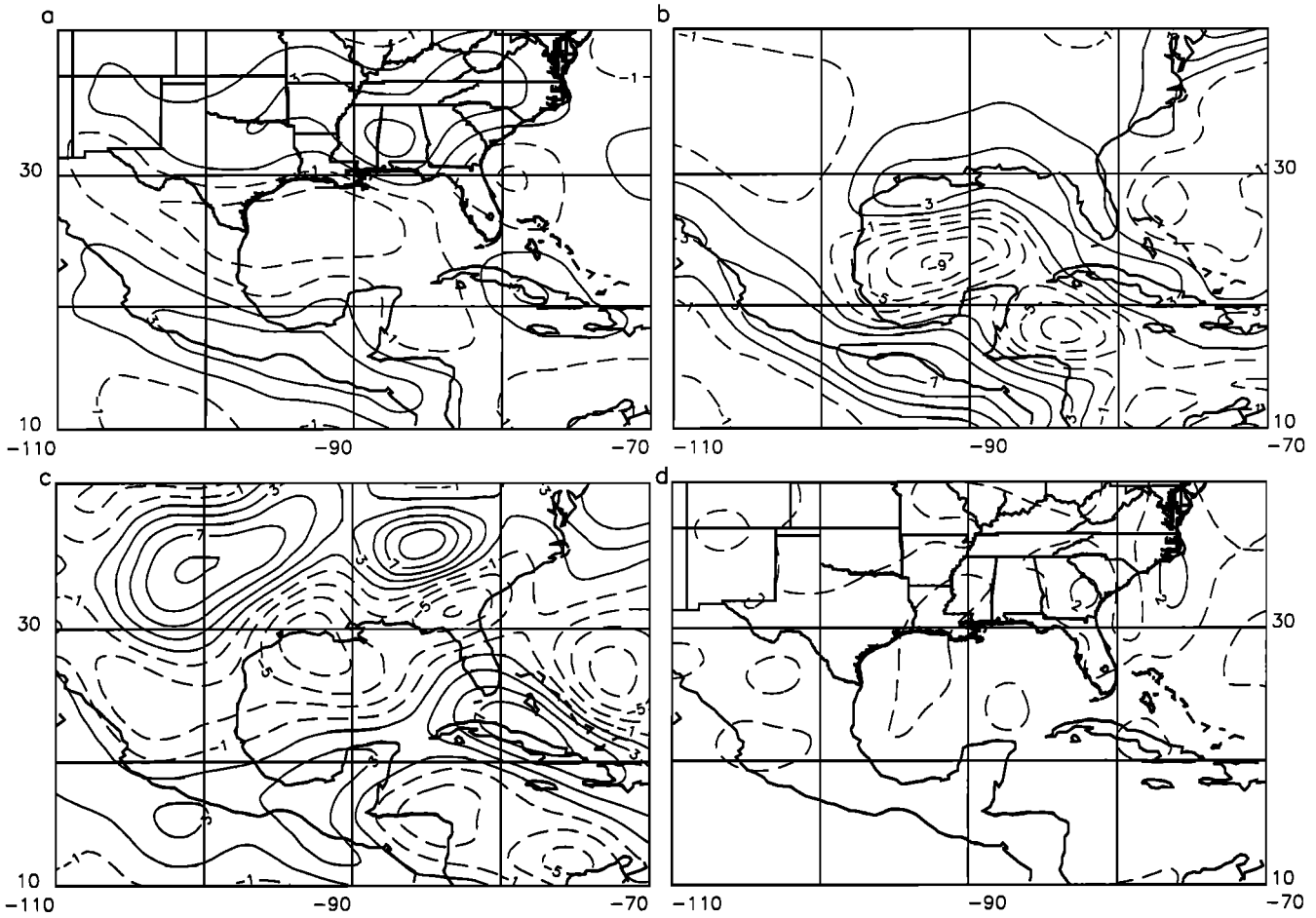

Figure 8. Maps showing fields (vertical Z) (a) calculated from the 3SMAC and (b) from the SEMM-0, (c) the observed vertical field, and (d) an estimate of the error in the observed total or scalar field. The contour interval is 2 nT except in Figure 8d where it is 1 nT. Negative values are dashed except in Figure 8d where the 1 nT error level is dashed. Figure 8d is extracted from *Arkani-Hamed et al.* [1994, Figure 8b]. All figures use a Mercator projection.

7) and Iceland (Anomaly 8). However, this statement is not universally true. Measured anomalies associated with the Walvis Ridge (WR) and Aguhlas Plateau (AP), for example, are not reproduced in the SEMM-0.

3. Some anomalies previously studied in lithospheric models may be due to the continent-ocean edge effect. Possible examples include the anomalies associated with the Aleutian and Mid-American trenches. In these cases, the possible SEMM effect should be examined as to its impact on models such as those by *Clark et al.* [1985] for the Aleutian arc and those by *Counil and Achache* [1987] and *Vasicek et al.* [1988] for the Mid-American trench. However, the SEMM effect may not be valid elsewhere, such as the elongate positive anomaly 9, near Japan with no corresponding measured anomaly. The SEMM model does not always correspond to the true ocean-continent contrast.

4. In some cases, the SEMM effect supports previous interpretations. For example, our results support the conclusion of *Bradley and Frey* [1991] that the negative anomaly in the Labrador Sea is due to the change in susceptibility and thickness at the continental-oceanic transition.

5. Modification With Data: SEMM-1

Following the scheme in Figure 2, the SEMM-0 is modified so that the resulting computed field, after removal of a degree 15 model and high-pass filtering, matches that of the combined POGO-Magsat anomaly map of *Arkani-Hamed et al.* [1994, Figure 8a]. Their POGO-Magsat anomaly map includes degrees 15-65. Because of a difference in the spherical harmonic representations used for the main and anomaly fields [*Arkani-Hamed et al.*, 1994], coefficients of degree n in the main field representation correspond mainly to coefficients of degree $n-1$ in the anomaly field representation. Degrees 14 and 15 are considered to be contaminated by the main field and hence are not used in the anomaly field representation [*Arkani-Hamed et al.*, 1994].

The resulting susceptibility times thickness, ζ, called SEMM-1, is shown in Figure 9 and Plate 1. To measure

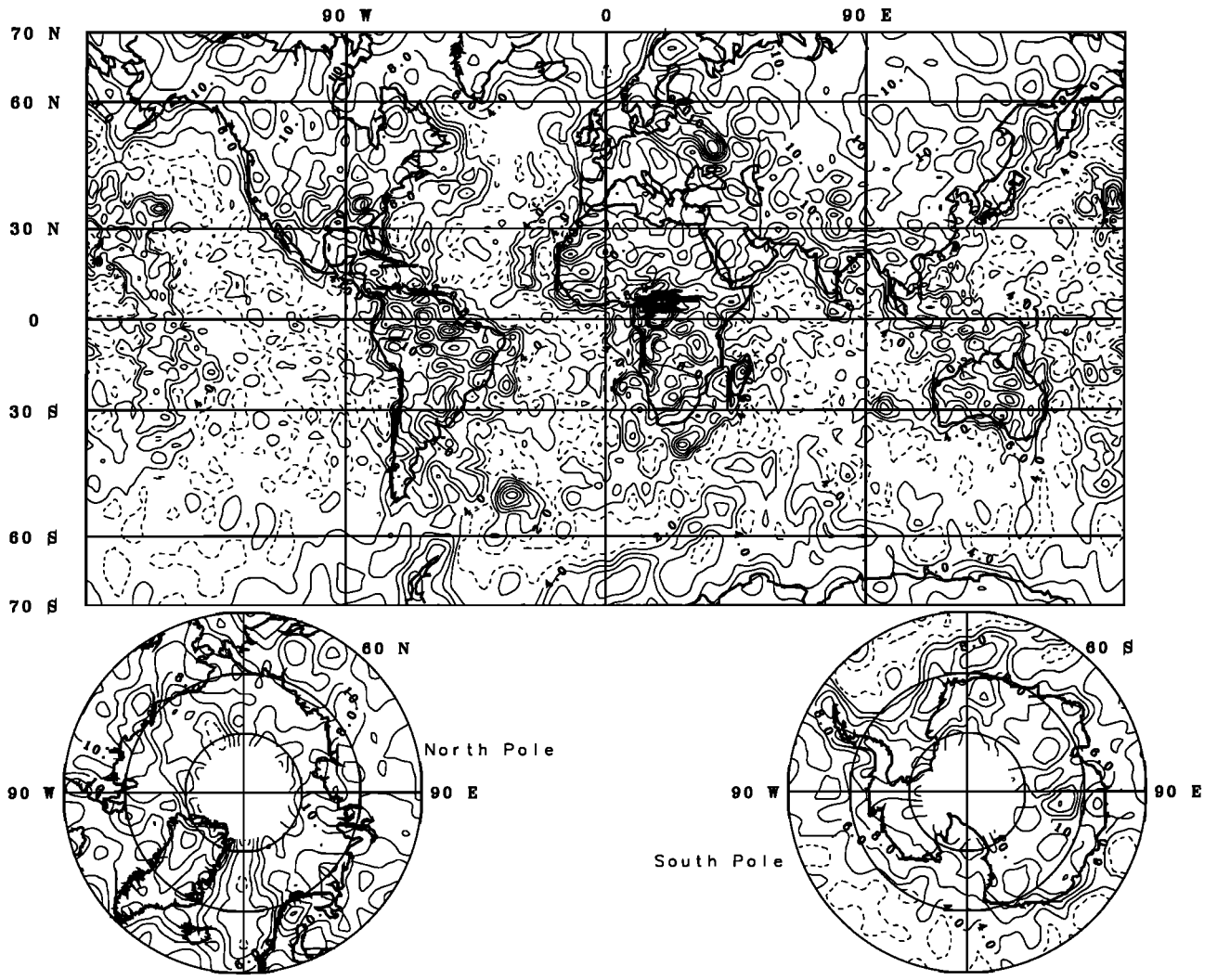

Figure 9. Susceptibility times thickness times 10 of the SEMM-1 model. Units are SI × km × 10. The contour interval is 2. The 0 and 2 contours are dashed. Mercator and polar stereographic projections.

the degree of fit of the anomaly field from the SEMM-1 to the field of Figure 5, a regression/correlation analysis was run between the two fields. This analysis yields correlation coefficients of 0.993 and 0.963 between measured and model ΔX and ΔZ anomalies, respectively, with corresponding slopes of 1.016 and 1.065. The measured anomalies, especially the ΔX anomalies, are reproduced well by the SEMM-1.

The largest misfits, in ΔZ, were confined to N-S bands in and near the polar regions. The differences can range up to 2 nT. Although these differences are enigmatic, they do reveal an inadequacy in the approximation of the along track filter as a north-south filter in these polar regions. Application of a more sophisticated filter that more closely approximates the actual processing of the satellite data produced major changes in SEMM-0 anomalies located near the northernmost extent of the Magsat orbit, especially anomalies 10, 11, 12, and 13 (Figure 4). Because of the instability of results in these polar regions, interpretation of these associated features is not warranted.

6. Error Analysis and Sensitivity to Initial Conditions

An interpretation based on the SEMM must take into account both errors in the observed data and how the final SEMM model depends upon the a priori initial conditions. As outlined in section 1, the observed data represent the common features of maps made from the POGO and Magsat satellite missions. *Arkani-Hamed et al.*[1994] assigned error estimates, or standard deviations, to their maps. The maps and associated error estimates (Figure 8d) used here are those made with the less stringent selection conditions because the more stringent selection conditions reject too much signal [*Langel*, 1995]. The error estimates are based on the scatter between the maps after they have been subjected to a degree correlation method [*Arkani-Hamed and Strangway*, 1986]. There are two types of errors that are unaccounted for in their analysis. The first type of unaccounted error is that which is common to the input POGO and Magsat maps. Because the in-

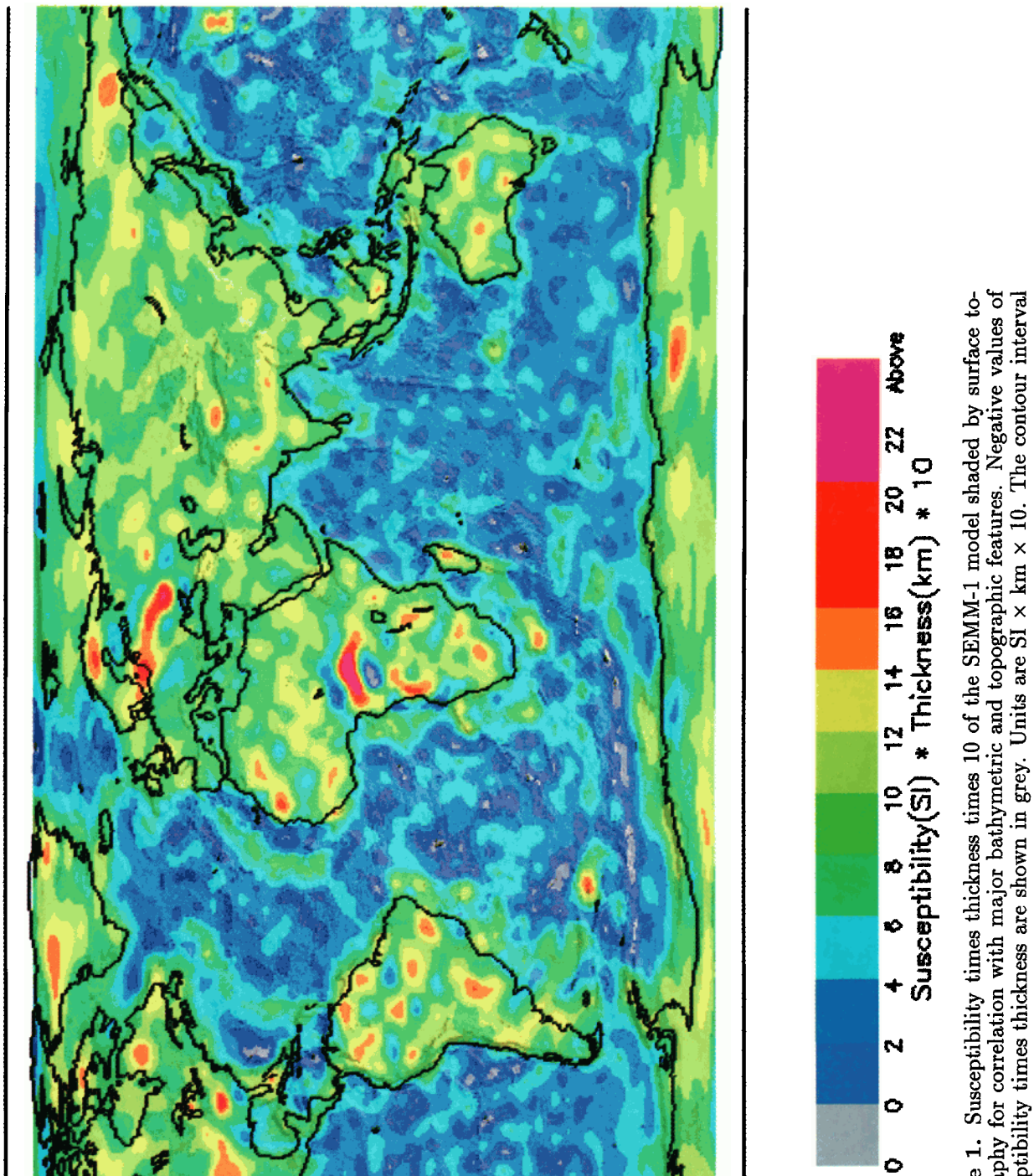

Plate 1. Susceptibility times thickness times 10 of the SEMM-1 model shaded by surface topography for correlation with major bathymetric and topographic features. Negative values of susceptibility times thickness are shown in grey. Units are SI × km × 10. The contour interval is 2. Null projection.

put are based on data collected at different epochs and local times, this type is error is assumed to be minimal. The second type of unaccounted error is a systematic underestimation of the magnitude of the crustal signal occurring as a consequence of the degree correlation method and the along-track filter. It was the opinion of *Arkani-Hamed et al.* [1994] that individual anomalies greater than 2 nT on the maps are reliable in position and, in most locations, are accurate in amplitude to within about 2 nT. Further examination of this question by *Purucker and Langel* [1996] has shown that individual anomalies greater than 1 nT are reliable in position. *Ravat et al.* [1995] found that the amplitude of the anomalies in maps made by *Cain et al.* [1990] were 20% to 60% larger than in the Magsat maps used by *Arkani-Hamed et al.* [1994]. *Cain et al.* [1990] did not utilize an along-track filter or the degree correlation method in deriving their map. Rather, they combine the dawn and dusk data and use careful hand selection to minimize the ionospheric contribution. A similar difference is noted by M.E. Purucker (Scalar anomaly maps over the United States from the comprehensive model (GSFC/CU(12/96)), available at http://denali.gsfc.nasa.gov/personal_pages/purucker/interests_comp.html, hereinafter referred to as Purucker, 1997) and *Purucker et al.* [1997] in their analysis of residuals to a model of the internal dynamo, ionospheric, and magnetospheric fields. These differences, and their implications for interpretations, will be explored further in section 7. Interpretation of the data will also be accompanied by a discussion of signal/noise ratios. Formal errors can be estimated using the covariance matrix of *Purucker et al.* [1996].

In order to quantify the dependence on the a priori initial conditions, several end-member variations of these conditions were used as starting models, i.e., alternative SEMM-0s. These starting models are distinguished from one another by the difference in the product of the susceptibility times thickness:

$$\Delta\zeta = s_c t_c - s_0 t_0 \tag{3}$$

where s_c and t_c are the susceptibility and thickness of the continental crust and s_0 and t_0 are the susceptibility and thickness of the oceanic crust. SEMM-0s which have the same $\Delta\zeta$ will produce identical magnetic fields because they have identical contrasts [*Runcorn*, 1975]. Consequently, aside from a level shift, SEMM-0s which have the same $\Delta\zeta$ will produce identical final SEMM models. The $\Delta\zeta$ of the nominal SEMM-0 is 0.72 SI km. To investigate parameter sensitivity, starting models are considered that have contrasts both larger and smaller than 0.72, and one which has a reversed contrast ($s_0 t_0 \geq s_c t_c$). The pertinent starting parameters (and what they might correspond to in thickness and susceptibility) are given in Table 1.

As a quantitative measure of sensitivity to changes in the model, spherical harmonic analyses were applied to the final version of the SEMM from each of these end-members and from the final SEMM starting with the nominal SEMM-0. The degree correlation coefficient, described by *Arkani-Hamed et al.* [1994], was then determined between each end member and the nominal model (Figure 10). Of importance is that both the end-member SEMMs and the nominal SEMM fit the satellite data equally well. Correlations for degrees 1-15 (Figure 10) are either at/near 1.0 (versions 2, 3, 4) or -1.0 (version 1) depending on a positive or negative value of $\Delta\zeta$. This reflects the a priori model which, for the low degree terms, is not changed by the processing leading to the final SEMM models. The end-members which are closest to the nominal SEMM, versions 3 and 4, exhibit degree correlation coefficients in excess of 0.95 between degrees 20 and 65. Between degrees 11 and 20, version 4 drops to a correlation of about 0.82 and then increases to 0.95. Between degrees 11 and 20, version 3 drops to 0.97. The end-member with the largest $\Delta\zeta$, version 2, also exhibits the poorest correlation. The large $\Delta\zeta$ of this model overwhelms the change which occurs between the SEMM-0 and the final SEMM, producing a relatively low correlation at higher degrees. Its correlation with the nominal SEMM drops to between 0.65 and 0.75 from degree 28 and up.

In summary, degrees 20 through 60 of all the SEMM models exhibit a strong correlation. As a quantitative measure of the changes to each spherical harmonic coefficient, the percent change of each coefficient relative to the nominal SEMM was calculated. Results of this comparison show that for each degree n, the $n = m$ coefficients are poorly determined, even in the degree range from 20 to 60. This is related to the near-polar orbit of the magnetic field satellite and the consequent difficulty of resolving long north-south trending features.

Another comparison of interest is a correlation and regression analysis between the nominal SEMM-1 and the end-member versions of SEMM-1 of that portion of the susceptibility times thickness variation determined by the satellite anomaly data. On the basis of Figure 10, such a comparison was made for degrees 17-65. The resulting intercepts were all zero indicating no zero offsets between the models compared. Table 2 summarizes the correlations and slopes. The correlations for versions 3 and 4 are greater than 0.97; those for the more extreme end-members are not as high, as would

Table 1. End-Member Versions of SEMM-0

Version	$\Delta\zeta$	Thickness t_c, km	Susceptibility s_c, SI	Thickness t_o, km	Susceptibility s_o, SI
1	-0.72	20	0.0015	15	0.05
2	4.92	50	0.1	4	0.02
3	1.25	40	0.033	3	0.02
4	0.22	19	0.02	4	0.04

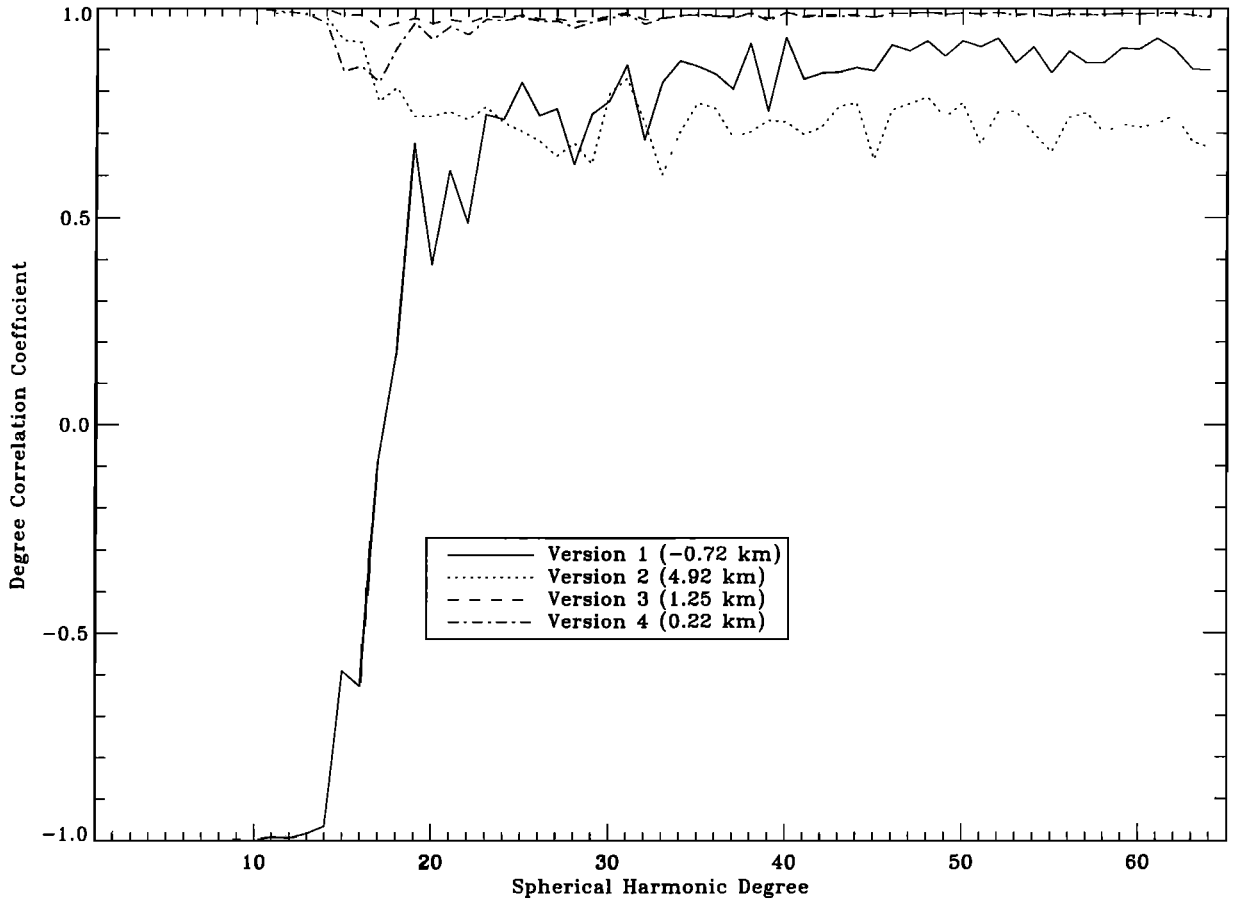

Figure 10. Degree correlation coefficients between the nominal SEMM-1 and four SEMM-1 versions determined with different end-member SEMM-0 starting models.

be expected from Figure 10, but are satisfactory. Slope values near 1.0 indicate that the amplitudes of the susceptibility times thickness are nearly equal.

Version 2 exhibits the worst correlation and the unrealistic slope value of 3.636. Examination of the plot of ζ from this version of SEMM-0 shows large gradients between ocean and continental regions, particularly in the north-south direction. North-south filtering of the resulting fields removes all control of the data over such features. It is concluded that this version is physically unrealistic and cannot be adjusted to fit both the data and give a realistic magnetization distribution.

While all end-members show reasonable correlation to each other, we have defined a limited model space that is consistent with our assumptions. Reasonable a priori conditions would span the $\Delta\zeta$ range between 0.22 and 1.25.

7. Application

The SEMM is intended to be more than simply an inversion of satellite magnetic anomaly data with a priori continent-ocean contrast. It can be used to guide and refine geologic and magnetic models and interpretations in the regions close to continental margins.

As mentioned in section 4.2, there remained a discrepancy between the 3SMAC model and the observation in the Gulf of Mexcio. Using the techniques outlined in this paper, we can determine how the model can be modified to fit the observations. Figure 11a shows the

Table 2. Correlation and Slope Comparison (Degrees 17-65) Between the Nominal SEMM-1 and End-Member Versions

SEMM-1 Version	$\Delta\zeta$	Correlation	Slope
1	-0.72	0.73	0.997
2	4.92	0.70	3.636
3	1.25	0.98	1.133
4	0.22	0.97	0.931

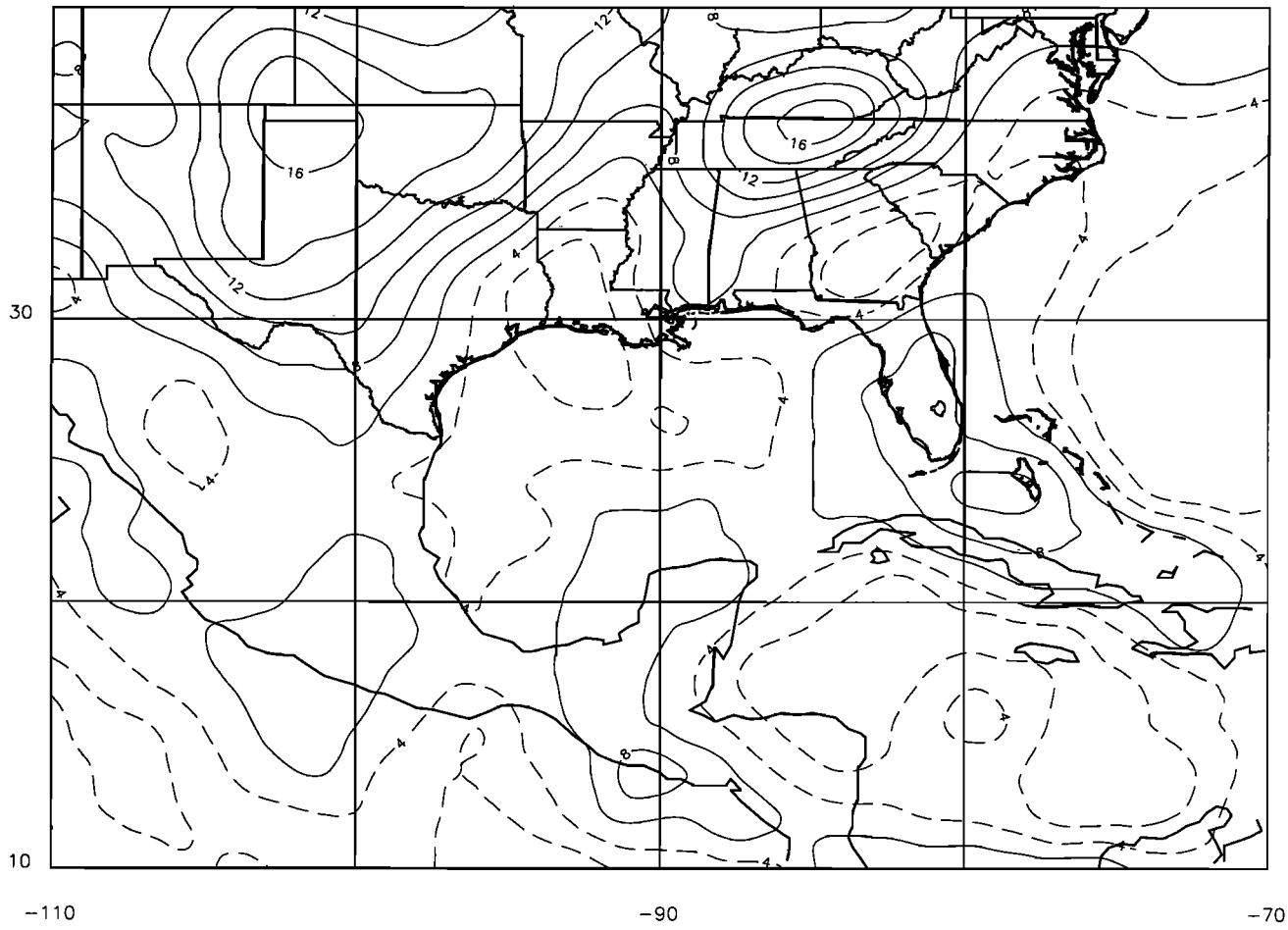

Figure 11a. Susceptibility times thickness times 10 based on the 3SMAC model over the Gulf of Mexico and surrounding region. Units are SI × km × 10. The contour interval is 2. The 4 and 2 contours are dashed.

modified susceptibility times thickness, ζ, based on the 3SMAC model and the observations. Because the minimum ζ is nearly coincident with the maximum sedimentary thickness (Figure 7c) we infer that the source of the magnetic anomaly low (Figure 8c) over the northernmost Gulf of Mexico is a decrease in the thickness of the magnetized layer rather than any decrease in the susceptibility in that magnetized layer. We can therefore calculate the thickness of the magnetized layer (Figure 11b) necessary for the observed anomalies. This thickness map, and the accompanying cross-section (Figure 12), can be interpreted to mean that a shallower Curie isotherm in the region of the thick sedimentary sequence removed an extra 5-20 km of magnetic crust. High heat flow, greater than 40° C/km, is observed in much of Louisiana and east Texas [*Smith and Dees*, 1982; *Nathenson and Guffanti*, 1988]. The presence of Cenozoic alkalic igneous rocks in the subsurface of northern Louisiana may provide a source of shallow radiogenic heat [*Smith and Dees*, 1982]. Salt deposits and domes of Jurassic age may also serve to modify the surface heat flow because of the higher thermal conductivity of salt [*Smith and Dees*, 1982]. However, the area of elevated heat flow is more extensive than can be explained by the known distribution of igneous rocks and salt deposits, leading *Nathenson and Guffanti* [1988] to state that the cause of the high gradients is enigmatic. Our observations suggest that the elevated heat flow persists at depth and has elevated the Curie point isotherm. Inasmuch as the tectonic regionalization is the coarsest element of the 3SMAC model, it should not be surprising that further refinement would modify this aspect of the model. The location of the minimum ζ is insensitive to the a priori model used. Note that the thickness map of Figure 11b was made on the assumption that the magnetic anomaly is caused by changes in the magnetic crustal thickness and not by changes in the susceptibility of the magnetized layer. While we have justified this assumption over the Gulf Coast region, the assumption fails over the Kentucky [*Mayhew et al.*, 1982] and central plains anomalies as evidenced by the associated excessive thicknesses (70+ km).

The inverse technique developed in this paper can be used to explore the consequences of the along-track filter used in the routine processing of satellite magnetic data. It is to be expected that interpretations will change with changing data and improvements in processing technique. However, the importance of this

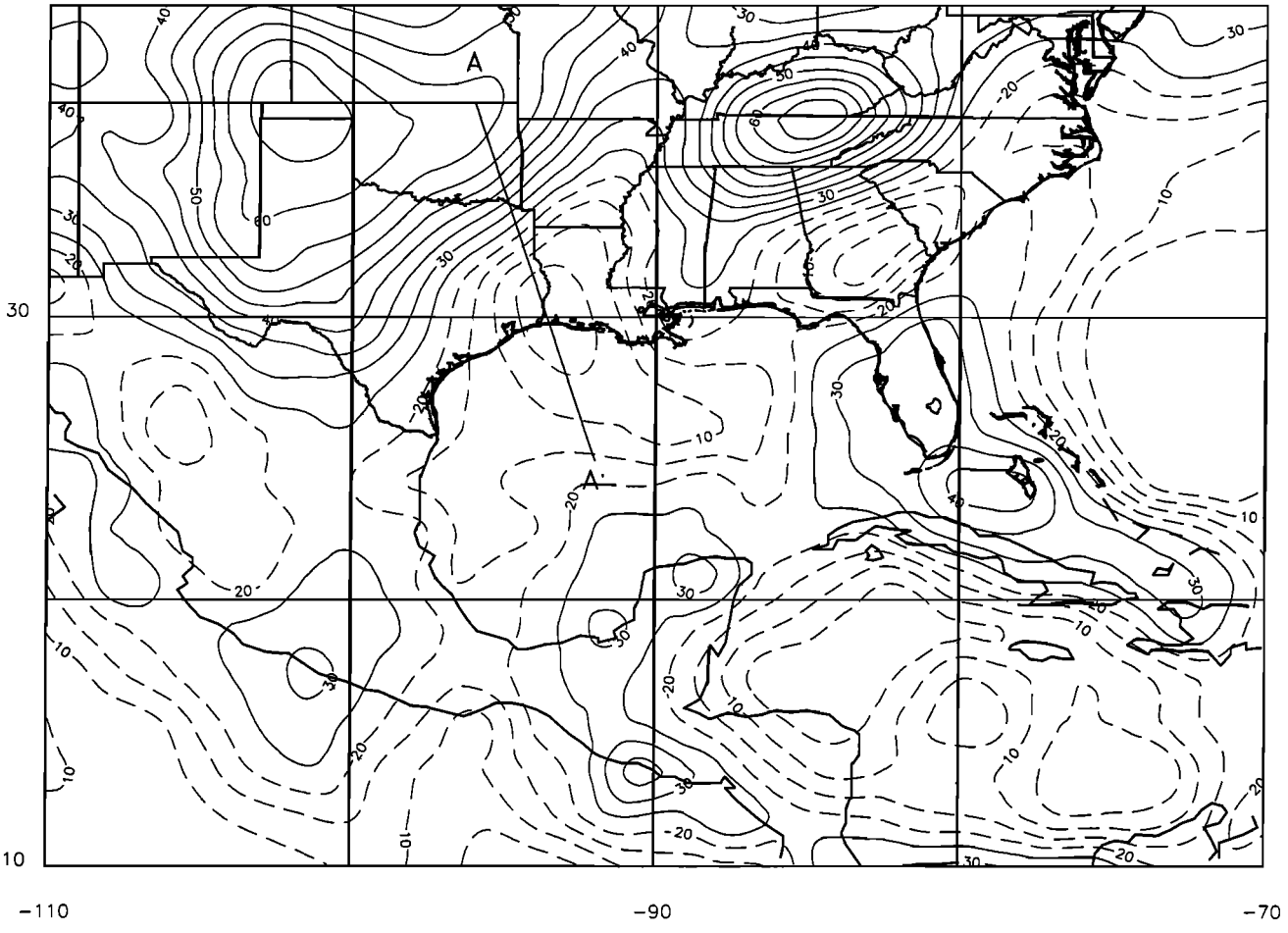

Figure 11b. Magnetic crustal thickness (km) based on the 3SMAC model and a susceptibility of 0.025 SI for continental areas and 0.04 SI for oceanic areas. The contour interval is 5. Thicknesses $\leq$ 20 km are dashed. The A-A' line locates the cross section of Figure 12.

study is to suggest an inverse technique which can be applied to both present and future data sets. As discussed in section 6, this filter has the effect of reducing anomaly amplitude and suppressing anomalies which are elongate in the north-south direction. Purucker (1997) has recently made available a new scalar anomaly map of the United States and surrounding area made without the use of the along-track filter. Transforming his scalar dawn field to a vertical field (Figure 13c), we can compare it to the 3SMAC (Figure 13a) and SEMM-0 (Figure 13b) predictions. The 3SMAC and SEMM-0 predictions differ from those shown in Figures 8a and 8b, respectively, because it is no longer necessary to apply a north-south filter to the model fields prior to comparing them with the observations. Several very interesting observations emerge from a careful study of these new maps. First, the center of the low in the new observations now overlaps the center of the low in the 3SMAC. Previously, the two lows had been separated by some 250 km. Second, the magnitude of the low has increased in both the observations (from -7 to -13 nT) and in the 3SMAC model (from -3 to -5 nT). The low in the observations has partially split into two lows, a broader, more intense low centered in the Gulf of Mexico and a narrower, less intense low centered over SW Louisiana and the adjacent Gulf of Mexico. The ζ predicted over the Louisiana region by the new observations is about 0.2 SI-km, unchanged from the previous SEMM-1 (Figure 11). This comparison provides greater confidence in our interpretation of an elevated heat flow at depth in this region. Note that the ζ predicted over parts of the Gulf of Mexico is now negative, suggesting either an area of extensive reversely magnetized oceanic crust or possibly a need to assign a higher ζ in the SEMM-0 to the oceanic crust.

The Kentucky anomaly whose source region is centered over Kentucky and Tennessee is also more intense in the anomaly map made without using the north-south filter, increasing from 9 to 19 nT (Figure 13c). The 3SMAC model now predicts a substantial (about 7 nT, Figure 13a) anomaly in this region. This 3SMAC model anomaly had previously been strongly suppressed by the application of the north-south filter (Figure 8a). The SEMM-0 predicts no substantial anomaly here. The difference between the 3SMAC and the SEMM-0 predictions may be related to the differences in the

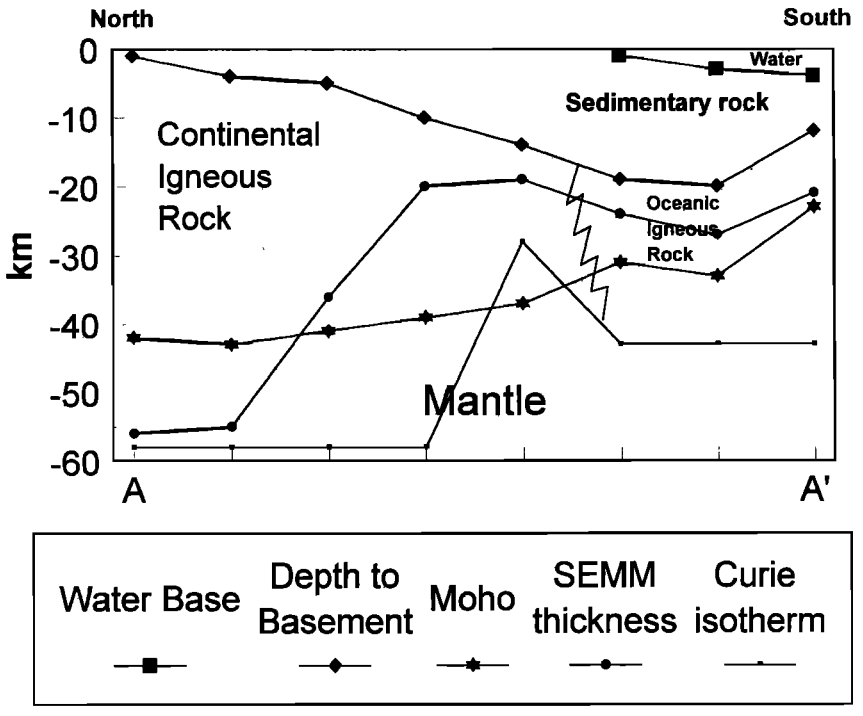

Figure 12. North-south cross section through the crust of the Mississippi River embayment and adjacent Gulf of Mexico. The cross section is located on Figure 7. Vertical exaggeration is 15:1. The depth to basement, Moho, and Curie isotherm are taken from the 3SMAC model. The SEMM thickness is deduced from the magnetic field observations as discussed in the text and is measured from the base of the sedimentary rock sequence.

thickness of the magnetic crust in the Florida region. The explanation of the Kentucky anomaly as partly an edge effect is worth further investigation.

8. Discussion

The absence of significant anomalies along the coasts of South America and Africa in the SEMM-0 (Figure 3b) is caused by the physics of the induction process (i.e., a factor of 2.75 difference in the magnitude of the magnetic field between the magnetic equator and pole). As mentioned in section 3.2, the only permanent magnetization considered in this paper is associated with the Cretaceous Quiet Zone. The equivalent source representation can be easily modified to solve for magnetizations in directions oblique to the main geomagnetic field and, in principle, can be combined with localized forward models when appropriate.

The SEMM-1 can be converted to a magnetization model in order to more easily compare the results with other studies. Assuming a thickness of 7 km for the oceanic crust (excluding oceanic plateaus and the Cretaceous quiet zones) and 40 km for the continental crust, the relation is

$$M = \frac{B_0 k}{\mu_0}, \tag{4}$$

where k is the susceptibility in SI units, M is the magnetization (A/m), B_0 is the inducing field in teslas, and μ_0 is the permeability of free space. The results are shown in Figure 14 for the continental and oceanic regions.

Harrison et al. [1986] note that the magnetizations required to produce many of the satellite measured anomalies are greater than expected. *Shive et al.* [1992] summarize estimates of magnetization and magnetic layer thickness from studies not only of satellite data but also of aeromagnetic data. The range of magnetizations they cite is 2-10 A/m, with 4 A/m a typical value. Magnetic layer thicknesses corresponding to these estimates vary from 10 to 50 km for continental areas, but generally from 25 to 40 km. They note that these magnetizations are several times higher than expected based on rock measurements. The location of the "missing" magnetization remains a problem for them. On the other hand, from a study of lower crustal xenoliths, *Wasilewski and Mayhew* [1992] conclude that mafic lower crustal rocks or basaltic mafic melts possess high induced magnetizations which can account for the aeromagnetic and satellite observations.

The continental magnetizations in Figure 14 are lower than most of those cited by *Shive et al.* [1992]. This decrease can be attributed to three factors. The first is related to the spherical harmonic content of the underlying anomaly map. *Harrison et al.* [1986] suggested that satellite anomaly maps might be contaminated by the presence of field from the core in spherical harmonic degrees 14-17. The results of *Arkani-Hamed et al.* [1994] and of *Ravat et al.* [1995] indicate that such contami-

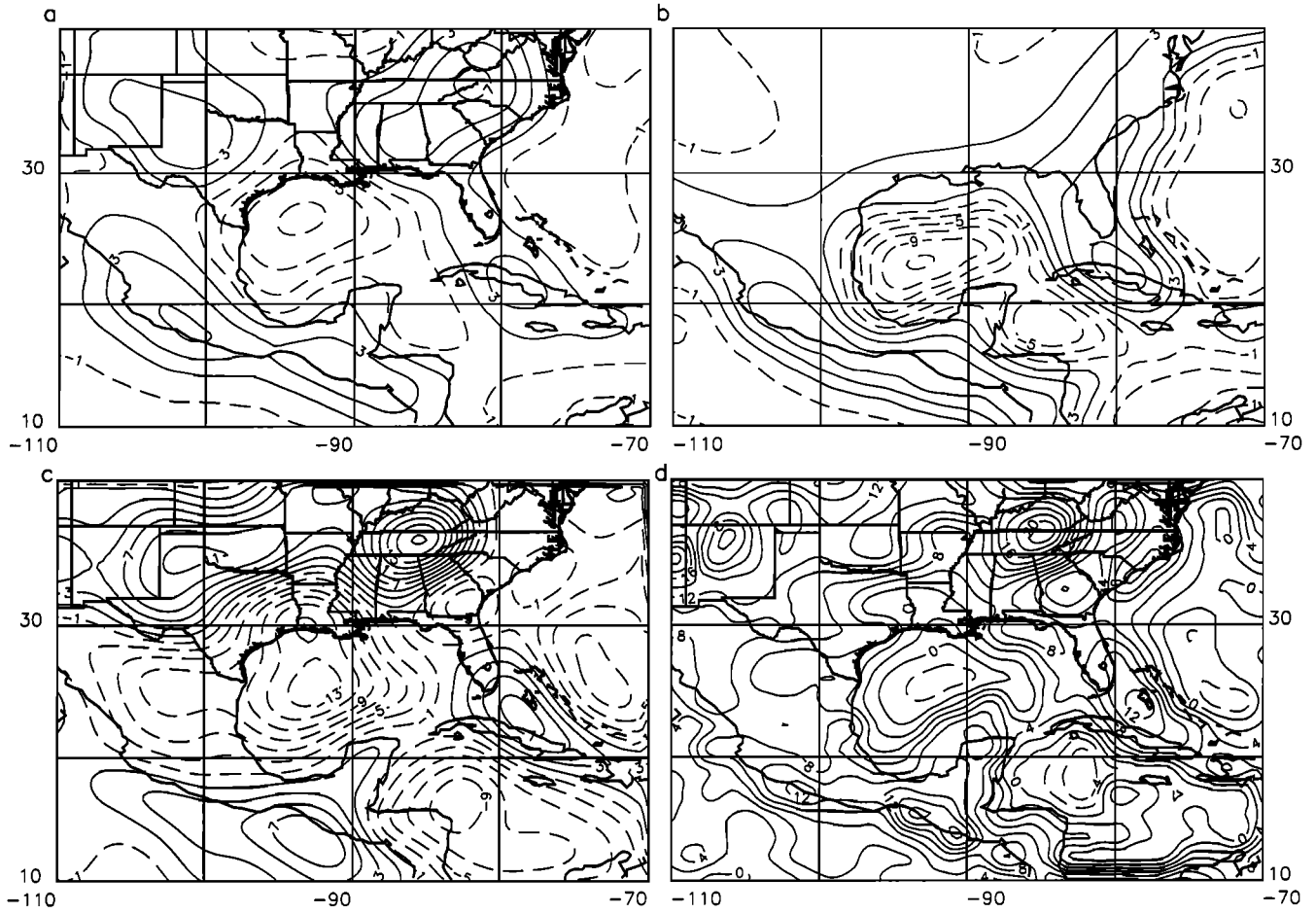

Figure 13. Maps showing vertical Z fields (a) calculated from the 3SMAC prior to north-south filtering, and, (b) from the SEMM-0 prior to north-south filtering, (c) the vertical field at dawn of Purucker (1998) made without resorting to an along-track filter, and (d) susceptibility times thickness times 10 based on the 3SMAC model over the Gulf of Mexico and the observations of Figure 13c. The contour interval is 2 nT except in Figure 13d, where it is 2 SI × km × 10. Negative values are dashed. All figures use a Mercator projection.

nation is likely at degree 14 and possible at degree 15. It seems unlikely that such contamination is present at degrees above 15. As noted in section 1, the combined POGO-Magsat map, upon which the SEMM-1 is based, includes degrees 15-65. Magnetization due to degree 14 in earlier maps is thus not present. The second factor is that the processing steps associated with the combined POGO-Magsat map are rather stringent. This results in a map with lower amplitude anomalies than in most previous maps. The third factor is the along-track filtering applied to the data to remove unmodeled ionospheric and magnetospheric fields. It is estimated that the combination of these three factors could have resulted in a decrease in magnetization of no more than a factor of 2, which would place the magnetization required in the middle to low range of the results cited by *Shive et al.* [1992].

9. Summary

An inverse technique has been developed that explores the possible effects of change in integrated magnetization at the continent-ocean boundary. Previous investigations using such a priori information have utilized only forward modeling procedures. No realistic simple model successfully predicts the anomalies over complicated margins such as the Gulf of Mexico. Modeling this margin in the most realistic way possible, using the 3SMAC model of *Nataf and Ricard* [1996], a better match to the observed anomaly pattern is achieved. This better match is achieved because the 3SMAC model takes into account the gradational character of this margin and the thick sediment accumulation over the Mississippi River delta. Using the techniques outlined in this paper, the model is modified to fit the robust POGO-Magsat satellite observations. The modifications suggest that a shallower Curie isotherm in the region of the thick sedimentary sequence removed an extra 5-20 km of magnetic crust. A Curie isotherm shallower than that predicted by the 3SMAC model is consistent with observations of elevated heat flow in Louisiana and Texas reviewed by *Morgan and Gosnold* [1989]. An additional contributing factor may be hydrothermal reactions occurring under the thick sed-

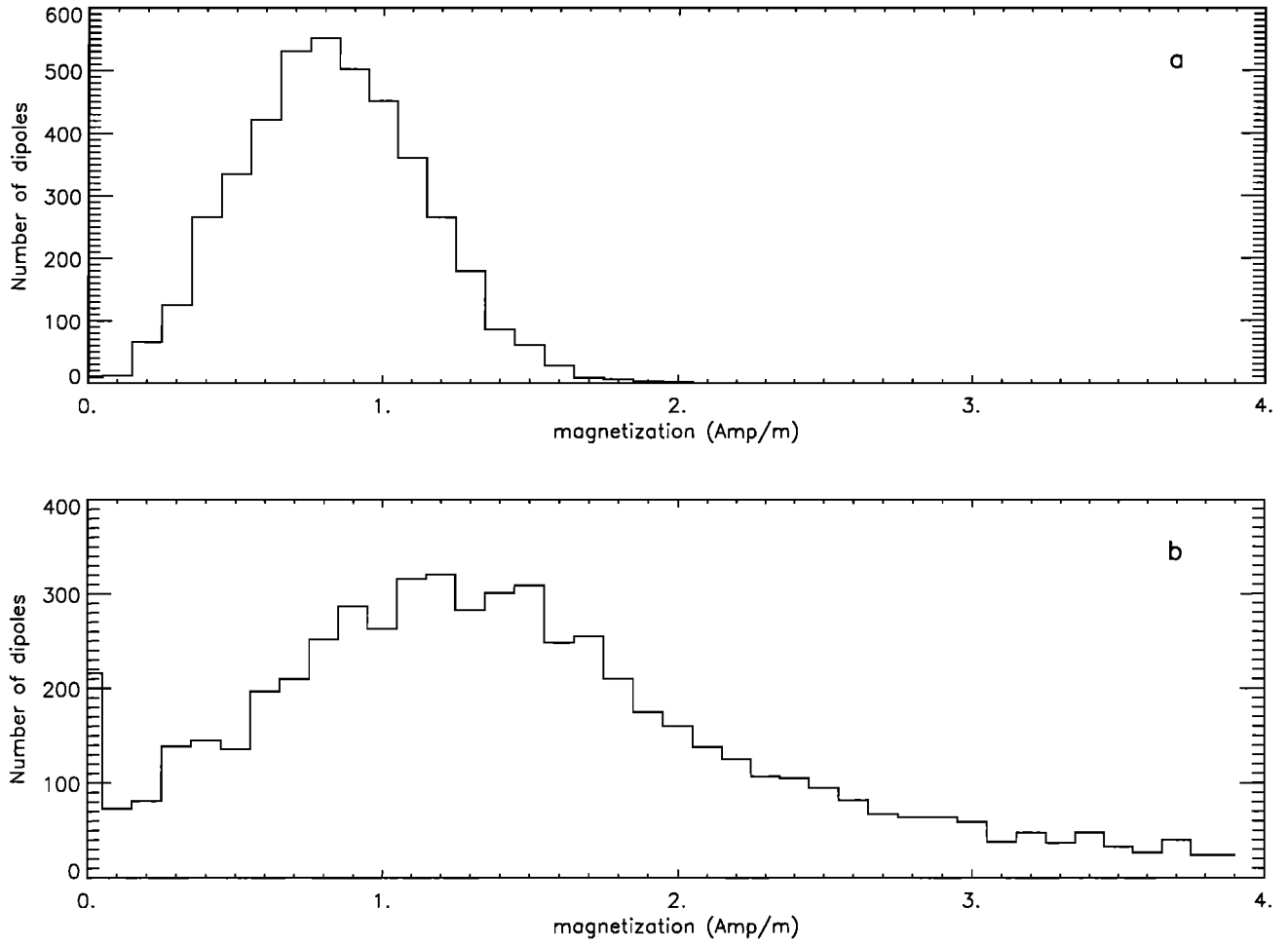

Figure 14. Histograms showing the distribution of magnetization (A/m) in (a) 40 km continental crust and (b) a 7 km oceanic crust.

imentary sequence [*Levi and Riddihough*, 1986]. These hydrothermal reactions may serve to leach the iron-titanium oxides and to decrease the susceptibility and magnetic remanence. Signal/noise ratios in excess of 5/1 are associated with the major magnetic anomalies in the Gulf Coast measured from satellite. Investigations of the dependence of the final model on the a priori information reveal that between degrees 20 and 65 the final models are almost identical for reasonable a priori conditions ($\Delta\zeta$ values between 0.22 and 1.25). Because the along-track filtering used in the routine processing of satellite anomaly data can substantially reduce anomaly intensity, the prudent interpreter will compare the results with and without filtering to ensure their validity.

10. Suggestions for Further Research

Comparison of the SEMM-0 anomaly map before and after along-track filtering (Figure 3b versus Figure 4) reveals both a decrease in the magnitude of the anomaly and the almost total removal of some significant north-south trending anomalies. Anomalies off the east and west coast of Australia and in the Bahamas are prominent examples of features suffering almost total removal. The along-track filter is necessary for the removal of unmodeled magnetospheric and quiet-day ionospheric magnetic fields because these unmodeled fields change between adjacent passes by tens of nanoTeslas. Recent work in simultaneous modeling of the core, quiet-day ionospheric, and magnetospheric fields [*Langel et al.*, 1996] holds out the promise of being able to isolate the crustal field without the necessity of first filtering the data along track. If this were accomplished, it would open the way for testing more of what are now a priori components of the SEMM.

Acknowledgments. This research was supported by NASA RTOP 579-31-01, for which we are grateful. We appreciate reviews by T. Hildenbrand, D. Ravat, R. Von Frese, and an anonymous reviewer. This paper is dedicated to the memory of Gene Shoemaker (1928-1997), teacher and mentor.

References

Arkani-Hamed, J., Magnetization of the oceanic crust beneath the Labrador Sea, *J. Geophys. Res.*, *95*, 7101-7110, 1990.

Arkani-Hamed, J., and J. Dyment, Magnetic potential and

magnetization contrasts of Earth's lithosphere, *J. Geophys. Res., 101*, 11401-11425, 1996.

Arkani-Hamed, J., and D.W. Strangway, Band-limited global scalar magnetic anomaly map of the Earth derived from Magsat data, *J. Geophys. Res.*, , *91*, 8193-8203, 1986.

Arkani-Hamed, J., R. Langel, and M. Purucker, Scalar magnetic anomaly maps of Earth derived from POGO and Magsat data, *J. Geophys. Res., 99*, 24075-24090, 1994.

Bradley, L.M., and H. Frey, Magsat magnetic anomaly contrast across Labrador Sea passive margins, *J. Geophys. Res., 96*, 161-168, 1991.

Cain, J.C., B. Holter, and D. Sandee, Numerical experiments in geomagnetic modeling, *J. Geomagn. Geoelectr., 42*, 973-987, 1990.

Carrizo, G.A.Y., Some aspects of the long term lithospheric evolution: Remanent magnetization of the ocean basins and deformation at convergent margins, Ph.D. thesis, Columbia Univ., New York, 1994.

Clark, D.A., Notes on rock magnetization characteristics in applied geophysical studies, *Bull. Aust. Soc. Explor. Geophys., 22*, 547-555, 1991.

Clark, S.C., H. Frey, and H.H. Thomas, Satellite magnetic anomalies over subduction zones: The Aleutian Arc anomaly, *Geophys. Res. Lett., 12*, 41-44, 1985.

Cohen, Y., Traitements et interpretations de donnees spatiales en geomagnetisme: Etude des variations laterales d'aimantation de le lithosphere terrestre, Ph.D. thesis, Univ. de Paris VII et Inst. de Phys. du Globe de Paris, June 1989.

Cohen, Y., and J. Achache, Contribution of induced and remanent magnetization to long-wavelength oceanic magnetic anomalies, *J. Geophys. Res., 99*, 2943-2954, 1994.

Counil, J.L., and J. Achache, Magnetization gaps associated with tearing in the central America subduction zone, *Geophys. Res. Lett., 14*, 1115-1118, 1987.

Counil, J.L. Y. Cohen, and J. Achache, The global continent-ocean magnetization contrast, *Earth Planet. Sci. Lett., 103*, 354-364, 1991.

Harland, W.B., R.L. Armstrong, A.N. Cox, L.E. Craig, A.G. Smith, and D.G.Smith, *A Geologic Time Scale*, 263 pgs, Cambridge Univ. Press, New York, 1989.

Harrison, C.G.A., H.M. Carle, and K.L. Hayling, Interpretation of satellite elevation magnetic anomalies, *J. Geophys. Res., 91*, 3633-3650, 1986.

Hayling, K., and C. Harrison, Magnetization modeling in the North and equatorial Atlantic Ocean using Magsat data, *J. Geophys. Res., 91*, 12423-12443, 1986.

Hinze, W.R., R. von Frese, and D. Ravat, Mean magnetic contrasts between oceans and continents, *Tectonophysics, 192*, 117-127, 1991.

LaBrecque, J.L., and C. A. Raymond, Seafloor spreading anomalies in the Magsat field of the North Atlantic, *J. Geophys. Res., 90*, 2565-2575, 1985.

Langel, R.A., Global magnetic anomaly maps derived from POGO spacecraft data, *Phys. Earth Planet. Inter., 62*, 208-230, 1990.

Langel, R.A., An investigation of a correlation/covariance method of signal extraction, *J. Geophys. Res., 100*, 20137-20157, 1995.

Langel, R.A., and W.J. Hinze, *The Magnetic field of the Earth's Lithosphere: The Satellite Perspective*, Cambridge Univ. Press, New York, 1998.

Langel, R.A., T.J. Sabaka, R.T. Baldwin, and J. Conrad, The near-Earth magnetic field from magnetospheric and quiet-day ionospheric sources and how it is modeled, *Phys. Earth Planet. Inter., 98*, 235-267, 1996.

Levi, S., and R. Riddihough, Why are marine magnetic anomalies suppressed over sedimented spreading centers?, *Geology, 14*, 651-654, 1986.

Marks, K.M., and D.T. Sandwell, Analysis of geoid height versus topography for oceanic plateaus and swells using nonbiased linear regression, *J. Geophys. Res., 96*, 8045-8055, 1991.

Mayhew, M.A., B.D. Johnson, and R.A. Langel, An equivalent source model of the satellite-altitude magnetic anomaly field over Australia, *Earth Planet. Sci. Lett., 51*, 189-198, 1980.

Mayhew, M.A., H.H. Thomas, and P.J. Wasilewski, Satellite and surface geophysical expression of anomalous crustal structure in Kentucky and Tennessee, *Earth Planet. Sci. Lett., 58*, 395-405, 1982.

Meissner, R., *The Continental Crust-A Geophysical Approach*, Int. Geophys. Ser., vol. 34, edited by W. L. Donn, 426 pp., Academic, San Diego, Calif., 1986.

Meyer, J., J. H. Hufen, M. Siebert, and A Hahn, On the identification of Magsat anomaly charts as crustal part of the internal field, *J. Geophys. Res., 90*, 2537-2541, 1985.

Morgan, P., and W.D. Gosnold, Heat flow and thermal regimes in the continental United States, edited by L.C. Pakiser and W.D. Mooney, *Geophysical Framework of the Continental United States, Geol. Soc. Am. Mem. 172*, 493-522, 1989.

Mueller, R.D., W.R. Roest, J.-Y. Royer, L.M. Gahagan, and J.G. Sclater, A digital age map of the ocean floor, *SIO Ref. Ser. 93-30*, 1993.

Nataf, H., and Y. Ricard, 3SMAC: An a priori tomographic model of the upper mantle based on geophysical modeling, *Phys. Earth Planet. Inter., 95*, 101-122, 1996.

Nathenson, M., and M. Guffanti, Geothermal gradients in the conterminous United States, *J. Geophys. Res., 93*, 6437-6450, 1988.

Petronotis, K.E., R.G. Gordon, and G.D. Acton, Determining paleomagnetic poles and anomalous skewness from marine magnetic anomaly skewness data from a single plate, *Geophys. J. Int., 109*, 209-224, 1992.

Purucker, M., The computation of vector magnetic anomalies: A comparison of techniques and errors, *Phys. Earth Planet. Inter., 62*, 231-245, 1990.

Purucker, M.E., and R.A. Langel, Source regions for satellite magnetic anomalies: Lithosphere, ionosphere, or core?, *Eos Trans. AGU*, , *77*(17) Spring Meet. Suppl., S85, 1996.

Purucker, M.E., T.J. Sabaka, and R.A. Langel, Conjugate gradient analysis: A new tool for studying satellite magnetic data sets, *Geophys. Res. Lett.*, , *23*, 507-510, 1996.

Purucker, M.E., T.J. Sabaka, R.A. Langel, and N. Olsen, The missing dimension in Magsat and POGO anomaly studies, *Geophys. Res. Lett., 24*, 2909-2912, 1997.

Ravat, D., R.A. Langel, M. Purucker, J. Arkani-Hamed, and D.E. Alsdorf, Global vector and scalar Magsat magnetic anomaly maps, *J. Geophys. Res., 100*, 20111-20136, 1995.

Row, L.W., III, D.A. Hastings, and P.K. Dunbar, TerrainBase: Worldwide digital terrain data; Documentation manual, key to geophysical records documentation 30, Beta Test Release 1.1, Nat. Oceanic and Atmos. Admin., Nat. Geophys. Data Cent., Boulder Colo., 1995.

Runcorn, S.K., On the interpretation of lunar magnetism, *Phys. Earth Planet. Inter., 10*, 327-335, 1975.

Sandwell, D. T., and K. R. MacKenzie, Geoid height versus topography for oceanic plateaus and swells, *J. Geophys. Res., 94*, 7403-7418, 1989.

Sawyer, D. S., R. T. Buffler, and H. R. Pilger Jr., The crust under the Gulf of Mexico basin, in *The Gulf of Mexico Basin, The Geology of North America*, vol. J, edited by A. Salvador, pp. 53-72, Geol. Soc. of Am., Boulder, Colo., 1991.

Shive, P.N., R.J. Blakely, B.R. Frost, and D.M. Fountain, Magnetic properties of the lower continental crust, in *Continental Lower Crust*, edited by D.M. Fountain, R. Arcu-

lus, and R.W. Kay, pp. 145-177, Elsevier, New York, 1992.

Smith, D.L., and W.T. Dees, Heat flow in the Gulf coastal plain, *J. Geophys. Res., 87*, 7687-7693, 1982.

Thomas, H.H., A model of oceanic basin crustal magnetisation appropriate for satellite elevation anomalies, *J. Geophys. Res., 92*, 11609-11613, 1987.

Toft, P.B. and J. Arkani-Hamed, Magnetization of the Pacific Ocean lithosphere deduced from Magsat data, *J. Geophys. Res., 97*, 4387-4406, 1992.

Vasas, S.M., R.G. Gordon, and K.E. Petronotis, New paleomagnetic poles for the Pacific plate from analysis of the shapes of Anomalies 33n and 33r, *Eos Trans. AGU, 75*, 203-204, 1994.

Vasicek, J.M., H.V. Frey, and H.H. Thomas, Satellite magnetic anomalies and the middle America trench, *Tectonophysics, 154*, 19-24, 1988.

Wasilewski, P.J., and M.A. Mayhew, The Moho as a magnetic boundary revisited, *Geophys. Res. Lett., 19*, 2259-2262, 1992.

R. A. Langel, 1008 Oak Pointe Court, Blacksburg, VA 24060. (email: langel@usit.net)

M. E. Purucker, Code 921, Geodynamics Branch, Goddard Space Flight Center, Greenbelt, MD 20771. (e-mail: purucker@geomag.gsfc.nasa.gov)

M. Rajaram, Indian Institute of Geomagnetism, Colaba, Bombay, India. (e-mail: mita@iigm0.ernet.in)

C. Raymond, Mail Stop 183-501, 4800 Oak Grove Dr., Jet Propulsion Laboratory, Pasadena, CA 91109. (e-mail:car@orion.jpl.nasa.gov)

(Received April 8, 1997; revised October 6, 1997;
accepted October 15, 1997.)